Title

Oral Regeneration in Stentor coeruleus: Cytoskeletal Patterning and Cell Cycle Control

ISBN

9798293851546

Author

Yan, Connie

Publication Date

2025-09-19

Peer reviewed|Thesis/dissertation

Oral Regeneration in Stentor coeruleus: Cytoskeletal Patterning and Cell Cycle Control

by
Connie Yan

DISSERTATION
Submitted in partial satisfaction of the requirements for degree of
DOCTOR OF PHILOSOPHY

in

Biochemistry and Molecular Biology

in the

GRADUATE DIVISION
of the
UNIVERSITY OF CALIFORNIA, SAN FRANCISCO

Approved:

DocuSigned by:
Todd Nystul
B55FB5CFA606452...

Todd Nystul
Chair

DocuSigned by:
Wallace Marshall

Wallace Marshall

DocuSigned by:
Dyche Mullins
E4FB70A20A7546F...

Dyche Mullins

Committee Members

ACKNOWLEDGEMENTS

I am grateful to have the support of my colleagues, friends, and family during this chapter of my scientific journey. Thank you to Dr. Wallace Marshall, my advisor, for his support and guidance through the many different ideas and directions that these projects steered towards. I thank my cohort for the tremendous amount of help and support navigating through the first year of our PhDs. I am grateful to my committee members, Dr. Todd Nystul and Dr. Dyche Mullins for providing guidance and meaningful discussions.

My decision to go to graduate school was greatly influenced by my post-bac advisor, Dr. Jay Parrish, and for that I thank him. I also am grateful for Dr. Wen-Yang Lin for her mentorship and her meticulous lab notes.

I am thankful for my parents for supporting me during my undergraduate years and highlighting the importance of education. I am grateful for my friends, who have supported me throughout this journey, especially those who encouraged me to apply for graduate school. To Tracy, who is no longer with us: I miss our friendship and your interest and enthusiasm in my research despite not having a background in science. I am incredibly grateful for my fiancé, Sean, who unconditionally supports me and continues to be my number one cheerleader. Lastly, I would like to thank my cats, Oderus Purrungus and Lizzy for being my emotional support, and a constant supply of entertainment, affection and companionship.

CONTRIBUTIONS

Chapter 3 contains work from a previously published paper:

Sood P, Lin A, Yan C, McGillivary R, Diaz U, Makushok T, Nadkarni AV, Tang SKY, Marshall WF. Modular, cascade-like transcriptional program of regeneration in *Stentor*. Elife. 2022 Aug 4;11:e80778. doi: 10.7554/eLife.80778. PMID: 35924891; PMCID: PMC9371601.

ABSTRACT

Oral Regeneration in *Stentor coeruleus*: Cytoskeletal Patterning and Cell Cycle Control

By

Connie Yan

Regeneration and wound healing are essential biological processes that restore cellular and tissue integrity following injury from external perturbations. Central to these processes is the interpretation of positional cues which include chemical or mechanical signals that instruct cells on what to rebuild and where to place structures. While the mechanisms underlying tissue and organ regeneration have been extensively studied, the molecular and spatial logic of regeneration at the subcellular level remains less understood. The giant single-celled ciliate *Stentor coeruleus* offers a powerful model for uncovering how cells interpret positional information to reconstruct complex intracellular architecture. With a highly polarized body plan, anterior-posterior axis, and an oral apparatus critical for feeding, *Stentor* can regenerate entire structures from fragments, provided a part of the macronucleus is intact.

Here, we explore how cytoskeletal patterning and cell cycle regulators support regeneration in *Stentor*. The oral apparatus regenerates at a stereotyped location along

the anterior-posterior axis, guided by visible cortical landmarks such as pigmented stripes and organized arrays of cytoskeletal fibers. We find that Sfi1 family proteins, which scaffold centrin-based cytoskeletal assemblies, are upregulated during regeneration and are essential for both oral primordium formation and contractility. RNAi-mediated depletion of Sfi1 genes impairs regeneration and anterior-posterior centrin patterning, suggesting that Sfi1 proteins establish cytoskeletal polarity necessary for morphogenesis. These proteins are recruited in a temporally ordered manner to the regenerating oral primordium, linking gene expression timing with spatial organization.

Moreover, we show that regeneration utilizes components of the canonical cell cycle. Using transcriptional and phosphoproteomic analyses, we identify upregulation of cell cycle regulators including E2F, CDK4, Rb, and cyclins during regeneration. Inhibition of CDK4 with the drug Palbociclib disrupts this pathway and suppresses regeneration, indicating that CDK4-mediated phosphorylation of Rb and subsequent activation of E2F target genes is required. Interestingly, the morphological stages of regeneration mirror those seen during cell division, including macronuclear condensation and elongation, suggesting shared regulatory mechanisms. Our results raise the possibility that regeneration in *Stentor* reflects a partial redeployment of the developmental program associated with cell division.

Together, our findings reveal that *Stentor* regeneration depends on the integration of cytoskeletal patterning with conserved cell cycle signaling pathways. This model system provides insight into how cells use positional cues and multifunctional molecular machinery to rebuild complex structures with spatial precision. Our work highlights the

convergence of regeneration and cell cycle regulation as a general principle of morphogenesis, even at the level of a single cell.

TABLE OF CONTENTS

CHAPTER 1: INTRODUCTION *1*

CHAPTER 2*:* SPATIOTEMPORAL CONTROL OF REGIONALIZED CENTRIN PATTERNING BY REGIONALIZED SFI1 ..... *11*

2.1 Abstract **11**

2.2 Introduction **12**

2.3 Results **19**

2.4 Discussion **45**

2.5 Materials and Methods **56**

2.6 Supplementary Figures **63**

CHAPTER 3: CELL CYCLE MACHINERY IN STENTOR REGENERATION *68*

3.1 Abstract **68**

3.2 Introduction **70**

3.3 Results **73**

3.4 Discussion **89**

3.5 Materials and Methods **94**

CHAPTER 4: DISSERTATION DISCUSSION *97*

4.1 Sfi1's role in centrin patterning and regeneration **97**

4.2 Future directions in the study of regeneration triggers.....98

REFERENCES *115*

LIST OF FIGURES

Figure 1.1: Stentor morphology.....4

Figure 1.2: *Stentor* oral regeneration cell division 8

Figure 2.1: Centrin is highly conserved 20

Figure 2.2: Centrin patterning in *Stentor* 22

Figure 2.2: Sfi1 in *Stentor coeruleus* 23

Figure 2.3: Sfi1 localization in *Stentor* 28

Figure 2.4: Centrin patterning in Sfi1 knockdown.....33

Figure 2.5: Sfi1 plays a role in *Stentor* regeneration 37

Figure 2.6: Role of Sfi1 in contractile machinery 42

Figure 2.7: Peptide block of Sfi1-1, Sfi-2, and Sfi1-3 antibodies.....63

Figure 2.9: RNAi knockdown validation of each Sfi1 antibody. 64

Figure 2.10: Representative fluorescence images of each Sfi1 antibody 65

Figure 2.11: NHS-Ester stains Sfi1 structures 65

Figure 2.12: Re-establishment of Sfi1 lateral bands during regeneration.. .66

Figure 3.1: A sender-receiver model for oral primordium formation..... 75

Figure 3.2: E2F is required for regeneration.....76

Figure 3.3: E2F RNAi have decreased proliferation. 78

Figure 3.4: Area of flattened cells 79

Figure 3.5: Palbociclib treated cells do not maintain a primordium..... 80

Figure 3.6: E2F RNAi and Palbociclib treated cells exhibit similar phenotypes..... 82

Figure 3.8: Time course of Edu incorporation during regeneration.……85

Figure 3.9: E2F knockdown cells do not synthesize more DNA ……85

LIST OF TABLES

Table 2.1: Predicted Sfi1 in *Stentor*. 27

Supplementary Table 2.2 List of RNAi construct primers 67

Table 3.1: E2F pathway genes downregulated in Palbociclib treated cells . 88

LIST OF ABBREVIATIONS

CaM – calmodulin

CDK – cyclin dependent kinase

HPS – hours post shock

ICL – infraciliary lattice

MAC – macronucleus

MAPK – mitogen activated protein kinase

Rb – retinoblastoma protein

SPB – spindle pole body

CHAPTER 1: INTRODUCTION

Regeneration and wound healing are hallmarks of life and are fundamental for tissues and cells to regain their integrity and functionality after injury from external perturbations. A critical component of these processes involves the interpretation of positional cues, which guide cells in reconstructing the appropriate structures in the correct spatial context. Cells use positional cues which may be in the form of chemical gradients or mechanical signals to know what structures they need to build and where to place them. If these cues are disrupted, or abnormalities occur in spatial patterning, structures may develop to be incorrectly placed or malformed. For instance, in planarian regeneration, Wnt signaling is increased in posterior regions that need to regenerate a tail. If Wnt is inhibited in the posterior, a head will regenerate in the place of a tail, showing how positional cues can determine polarity [1]. Such developmental processes of axiation, patterning, and morphogenesis have been extensively studied on an organismal or tissue level, but much less so on a subcellular level. Yet cells have complex shapes and forms which are usually essential for their function, as well as intracellular patterning which ensures that components such as organelles are distributed correctly within the cell. Spatial and temporal organization of proteins within cells can also encode information about the cell's geometry and developmental stage.

How do these cells organize themselves spatially and how is this organization recreated or restored during growth and regeneration? The giant single cell ciliate *Stentor coeruleus* is a classical model system for patterning, regeneration, and morphogenesis

[2], [3]. *Stentor coeruleus* is large, trumpet-shaped and up to 1mm in length, with a highly complex body plan **(Figure 1.1)** and a wide range of behaviors, including the ability to learn, contract in response to stimuli, and regenerate [2], [4], [5]. At its anterior is its oral apparatus, which consists of the membranellar band and mouth or gullet. The membranellar band is composed of clusters of specialized cilia used for feeding. Along its body are pigmented blue stripes whose width varies in a stereotyped manner, decreasing from wide to narrow stripes as a function of longitudinal angle. The region where the narrowest and widest stripes meet functions as the oral primordium site during oral regeneration and cell division. At this site, when a cell begins to divide or regenerate a new oral apparatus, basal bodies will assemble and assemble into a primordium, which organizes itself along the cell body. It will curl at the posterior of the primordium to form the gullet and then migrate to the anterior of the cell or in the case of cell division it becomes the new head on the old body. While *Stentor* are able to regenerate from any given part of the cell, the oral apparatus is the most complex and critical structure that the cell is required to have to survive [2], [6]. Because the primordium grows along the side of the cell along the cortical structures that run from the anterior to the posterior of the cell, there may be some kind of cytoskeletal support for the primordium during regeneration.

The organization of cortical structures in *Stentor coeruleus* exhibits a pronounced and highly stereotyped anterior-posterior polarity, reflecting the spatial organization of underlying cytoskeletal networks that are critical for the cell's structural integrity and regenerative capability. The cortex of *Stentor* is composed of two distinct but integrated cytoskeletal systems. One is a microtubule-based framework that maintains the overall

shape and polarity of the cell, and the other is a centrin-rich network composed of EF-hand domain proteins. These centrin-family proteins form a dense, branched meshwork in the anterior portion of the cell and transition into long, thick contractile bundles known as myonemes in the posterior half. This compartmentalized organization suggests functional regionalization along the body axis, likely linked to both morphogenetic and behavioral processes.

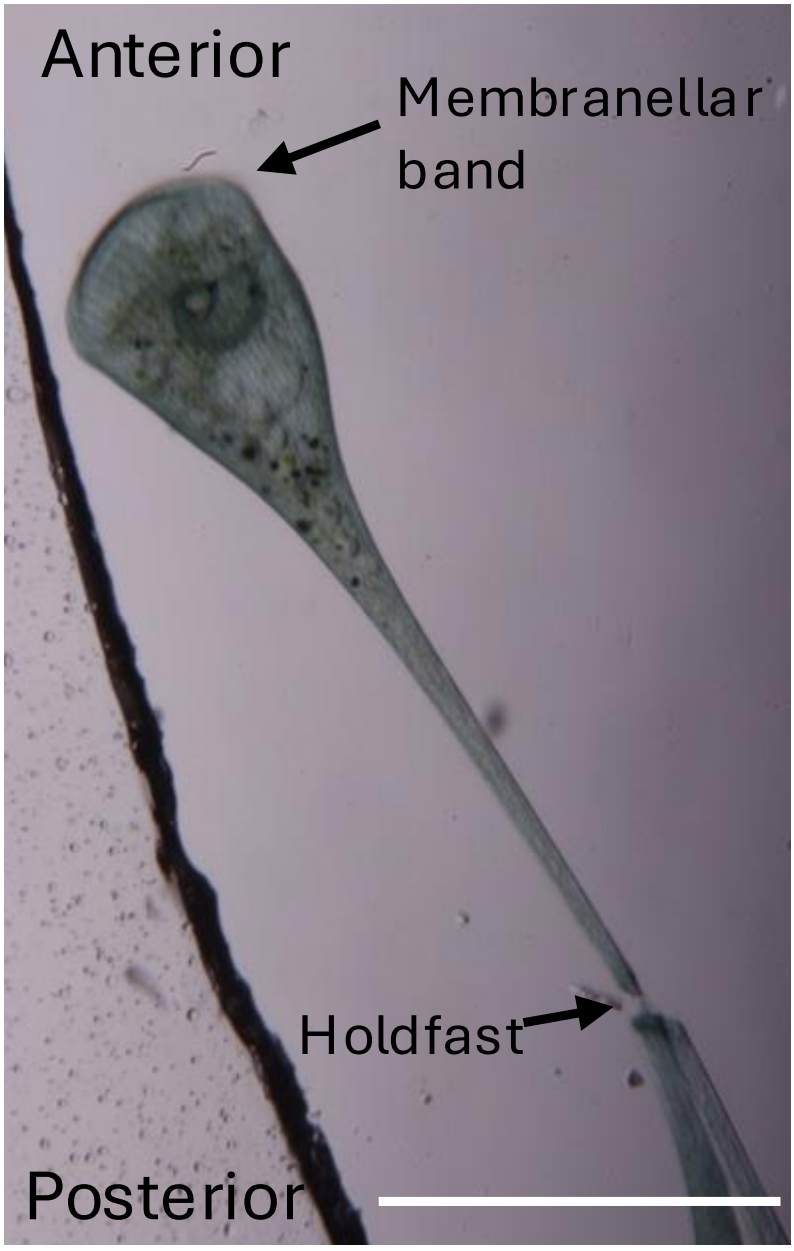

Figure 1.1: Stentor Morphology. Brightfield image showing the general morphology of *Stentor* in its extended state, noting the key features of the anterior and posterior. The membranellar band, a feeding organelle consisting of clusters of specialized cilia sits at the anterior of the cell. The posterior stalk-like portion of the cell terminates at the holdfast, used for attaching to substrate. The stalk-like part of the cell can undergo rapid contraction. All following *Stentor* images are oriented with the membranellar band at the anterior and holdfast at the posterior. Scale bar 100um.

Classical microsurgical experiments highlight the importance of cytoskeletal structures. In grafting experiments, the transplantation of an oral primordium, a structure that normally develops in response to injury or during cell division, into a region of the cell that does not typically initiate morphogenesis was sufficient to induce a full regenerative response [7]. These experiments demonstrated that cortical disruptions alone could serve as instructive cues, potentially acting as a mechanical or positional signal to trigger regeneration. This led to the hypothesis that cortical rows themselves, which align microtubules and centrin-based structures, play an instructive role in defining sites of morphogenetic activity.

A key molecular player in this process appears to be the Sfi1 protein family, conserved scaffolding proteins known to facilitate the organization of centrin filaments across eukaryotes. In ciliates, including *Stentor*, Sfi1 also supports the structural integrity of myonemal systems, which are central to the contractile behavior of these cells. In our studies, a subset of Sfi1 homologs was found to be transcriptionally upregulated during regeneration, indicating a regeneration-specific function beyond contractile roles. These Sfi1 proteins appear to reinforce anterior-posterior cytoskeletal asymmetries, as RNAi-mediated depletion results in a breakdown of regional centrin patterning.

Functionally, this loss of patterning correlates with severe defects in regeneration. Cells with reduced Sfi1 expression often fail to regenerate their oral apparatus, with early-expressed Sfi1 isoforms being especially essential for the initiation and elongation of the oral primordium. Our temporal analysis further reveals that Sfi1 proteins are not recruited to the regeneration site simultaneously but rather, their appearance at the regenerating primordium follows a sequential pattern that mirrors their transcriptional

activation and the stages of morphological development. This spatiotemporal orchestration suggests that Sfi1 isoforms are not merely structural but may provide instructive cues to guide the formation and orientation of new cortical structures.

In addition to defects in morphogenesis, we observe contractile deficiencies in some Sfi1 knockdown cells, where they either fail to contract in response to stimuli or exhibit incomplete contraction. This implies a dual role for Sfi1 proteins in both mechanical responsiveness and structural regeneration. Overall, these findings highlight the importance of regionally and temporally regulated cytoskeletal scaffolding in regeneration. They provide compelling evidence that the spatial localization and temporal dynamics of proteins such as Sfi1 can encode positional information and mechanical functionality, thereby coordinating the reconstruction of complex intracellular architectures within a single cell.

How do cells know when they need to regenerate missing parts? Tartar has proposed that *Stentor* cells exist in two contrasting cell states: “activation” where the whole cytoplasm is involved in supporting primordium formation, and “inhibition” which blocks or counteracts processes of cell differentiation [2]. How can we biochemically characterize these states? A transcriptional analysis of the regeneration time course in *Stentor* produced candidate genes which are differentially expressed during regeneration [8], [9]. Those that are upregulated early on in regeneration may function as early signaling proteins that trigger the downstream expression of subsequent regeneration genes. Among these genes are canonical cell cycle genes, including Aurora kinases [10], CDKs, cyclins [8], [11] and the transcription factor E2F [8]. E2F was identified as a potential regulator of oral regeneration based on the expression pattern

of its predicted target genes. In cycloheximide experiments, SteCoe_12750, an E2F homolog, is still upregulated during regeneration even when translation is poisoned, but its targets are not upregulated [8]. This suggests that E2F may act early on in the regeneration pathway to trigger subsequent signaling cascades. Canonically, E2F is a transcriptional regulator of G1 to S progression in the cell cycle, where E2F-DP1 complex is bound by retinoblastoma protein (Rb), inhibiting transcription. In G1 progression to S phase, cyclin dependent kinase 4 (CDK4) will phosphorylate Rb, releasing it and allowing for transcription. E2F is upregulated in early stages of *Stentor* oral regeneration [8]. Interestingly, the process of *Stentor* regeneration and cell division share morphologically similar steps **(Figure 1.2).** First, basal bodies assemble at the oral primordium site, then the basal bodies eventually form an oral primordium which elongates along the cell. The cell elongates while the oral primordium curls upward at the posterior end to form a new buccal cavity or gullet and finally migrates to the anterior of the progenitor cell to the normal position occupied by the membranellar band, while the proter cell with the old membranellar band buds off the top of the opisthe cell. Besides growing a new oral apparatus, dividing and regenerating cells also undergo morphological changes in their macronuclei. *Stentor* cells have a long, nodular macronucleus that resembles beads on a string. In division, it condenses and re-elongates, then separates evenly into the two daughter cells [2]. In regeneration, separation of the macronucleus is not necessary, yet the macronucleus still undergoes these dramatic shape changes. This paradigm of regeneration and division offers a valuable model for studying the underlying molecular mechanisms that regulate regeneration, development and positional patterning of complex structures.

Stentor cells are polyploid [12] and binucleate with an atypical cell cycle. In a canonical cell cycle, cells are in a G0 arrest phase, grow in G1, and progress to S phase after passing a number of checkpoints. This is followed by G2 and mitosis where the cell evenly divides into two. *Stentor* cells divide asymmetrically, and are constantly synthesizing DNA, thus largely remain in interphase [13].

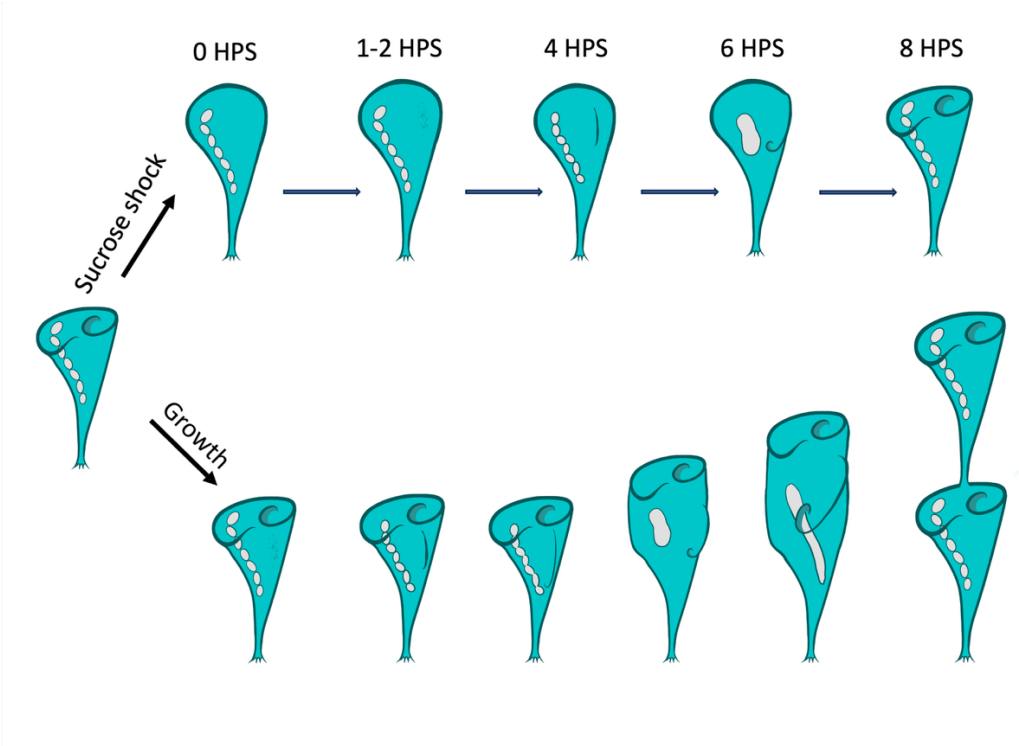

Figure 1.2: *Stentor* oral regeneration cell division. These processes share morphological similarities. Oral primodium formation and nuclear compaction are mirrored in both cases.

Stentor cells divide every 2-3 days [2] and cannot easily and reliably be synchronized, thus E2F's role in the *Stentor* cell cycle is unclear. However, because the morphological steps of forming a new oral apparatus appear identical to the morphological changes that occur during cell division [2], it is possible that cell cycle machinery may help

regulate the timing of regeneration. This highlights a question in the biology of regeneration of whether regeneration is a distinct process, or if it reflects a re-activation of development?

To understand the role of E2F in regeneration, we use RNAi to knockdown E2F and initiated regeneration with a sucrose shock. In these E2F RNAi cells, the oral primordium formed normally after sucrose shock but failed to progress or be maintained, such that after 8 hours, many of the cells were missing their oral primordium or had an incomplete OA [8]. Similarly, we tested the CDK4/6 inhibitor Palbociclib, which produced an even stronger phenotype, where most cells did not maintain a primordium by 8 hours post shock. When Palbociclib is added earlier in regeneration, the regenerative capacity decreases, indicating that CDK4 is likely to be important for the early stages of regeneration. We also perform bulk RNA sequencing on Palbociclib treated cells induced to regenerate with a sucrose shock. Since Palbociclib inhibits CDK4 from phosphorylating Rb, we expect to see downregulation of downstream components of the E2F pathway. Indeed, we find downregulation of cell cycle genes including Rb, CDK4, and cyclins. Additionally, we performed phosphoproteomics on Palbociclib treated cells one hour post sucrose shock to look at early phosphorylation events that may be important for initiating the signaling cascade that triggers regeneration. We find phosphorylation changes in a MAP kinase, as well as a cyclin, which may act upstream of CDK4.

In *Tetrahymena*, another ciliate, the expression profile of two E2Fs during cell division appear similar to that of E2F in *Stentor* regeneration [14]. However, in *Tetrahymena*, one E2F acts as a repressor, and the other acts as an activator. Is the E2F that we've

identified from the transcriptional program of regeneration a repressor or an activator? To answer this, we look at cell size, proliferation, and Edu staining to look at actively synthesizing DNA. We find that cell size is not affected, proliferation is decreased in E2F knockdowns, and the pattern of synthesizing DNA during regeneration mirrors that of the *Tetrahymena* cell cycle. This indicates that the E2F isoform we have knocked down likely acts as an activator. While there is much more to be discovered about cell cycle machinery and regeneration, this work provides an insight into how we might view regeneration as a modified cell cycle.

CHAPTER 2: SPATIOTEMPORAL CONTROL OF REGIONALIZED CENTRIN PATTERNING BY REGIONALIZED SFI1

2.1 Abstract

Patterning is fundamental to the development and maintenance of organisms, ensuring functional and structural organization. While patterning is well studied at the level of multicellular organisms, even single cells need to undergo morphogenesis and form spatial patterns. *Stentor coeruleus* is a large ciliate that has been a classical system for studying patterning and morphogenesis due to its distinctive shape and organization of easily visible cortical structures which show a clear localization along the anterior-posterior body axis. The cortex of *Stentor* is made of two cytoskeletal layers, one composed of microtubules, and one composed of a network of centrin-family EF hand proteins, which form a branched network in the anterior half of the cell and long thick bundles known as myonemes in the posterior half. Sfi1 family proteins scaffold the assembly of centrin filaments throughout the eukaryotes, and function as scaffolding proteins in myonemal contractile systems found in some ciliates. A set of Sfi1 proteins upregulated during regeneration in *Stentor* were found to have a role in maintaining anterior/posterior differences in centrin patterning. Loss of this distinct anterior-posterior patterning leads to defects in regeneration and contraction. Using RNAi-mediated knockdown of Sfi1 genes, we have found that cells fail to regenerate their oral

apparatus, with early expressed Sfi1 genes more critical for oral primordium (assembly of organized basal bodies that become the new oral apparatus) formation than those expressed later. Additionally, different Sfi1 proteins appear to be recruited sequentially to the growing primordium in an order that matches the time at which they are required for progression of regeneration. Contractile function is also affected in some Sfi1 knockdowns where cells fail to contract in response to a stimulus or do not fully contract. These findings suggest a model in which regionalized differences in patterning of cytoskeletal assemblies can be generated by regionalized localization of scaffolding proteins.

2.2 Introduction

In the context of organismal development, patterning refers to the process by which certain biological structures and functions emerge in a predictable, organized way. Such developmental processes such as axiation, patterning and morphogenesis have been extensively studied on an organismal or tissue level, but much less so on a subcellular level. Yet cells have complex shapes and forms which are usually essential for their function, as well as intracellular patterning which ensures that components such as organelles are distributed correctly within the cell. Spatial and temporal organization of proteins within cells can also encode information about the cell's geometry and developmental stage. But how do such patterns form within a single cell?

Ciliates provide an excellent opportunity for exploring cellular patterning, given their highly standardized cell shapes and readily observable surface structures that serve as clear landmarks for morphological processes [15], [16]. The entire surface of these cells is lined with parallel rows of cilia that run along the anterior-posterior axis with defined spacing between adjacent rows. Additionally, in many ciliates, structures such as the gullet or the contractile vacuole occupy well-defined positions along both the anterior-posterior and circumferential axes. In some instances, the formation of a distinct structure or process on the cell's surface is an expression of polarization or axiation. Polarization of the cytoskeleton plays a key role in providing a cell with positional information, for instance, actin filaments can guide the direction of movement in migrating cells, and the mitotic spindle helps position chromosomes in dividing cells [17]. Additionally, it has been shown that mRNA can be regionalized in ciliates and that microtubules may play a role in transport [18]. This spatial regulation of gene expression at the subcellular level suggests a sophisticated mechanisms by which even unicellular organisms can create and maintain internal asymmetries.

The giant ciliate *Stentor coeruleus* is a classical model system for studying regeneration, patterning and morphogenesis at a single cell level [2], [3]. *Stentor coeruleus* is large, up to 1mm in length, with a highly complex body plan and a wide range of behaviors, including the ability to learn, respond to stimuli, and regenerate [6], [19], [4].At its anterior is its oral apparatus, which consists of the membranellar band and mouth or gullet **(Figure 1.1).** The membranellar band is composed of clusters of specialized cilia used for feeding. Along its body are pigmented blue stripes whose width varies in a stereotyped manner, decreasing from wide to narrow stripes as a function of

longitudinal angle. The region where the narrowest and widest stripes meet functions as the oral primordium site during regeneration and cell division. Alternating in between these stripes are clear stripes lined with thousands of basal bodies, from which cilia extend, and which are also linked into parallel microtubule bundles that occupy the gaps between the pigment stripes [20], [21]. Two fiber systems are contained in the cortical stripes, one a cytoskeletal microtubule-based fiber and the other, a contractile, myonemal system [2] made of centrin [22].

Centrins are a highly conserved family of small EF-hand calcium binding proteins found across all eukaryotic lineages. They are primarily associated with fibrous structures at centrioles and basal bodies where they contribute to a diverse array of critical cellular functions, including centriole orientation, biogenesis and duplication, as well as nuclear export and DNA damage repair [23], [24], [25], [26], [27], [28]. Beyond these canonical roles, centrins also participate in the organization of microtubule-based cytoskeletal elements, such as the mitotic spindle and motile cilia [29], highlighting their diverse functional roles across both structural and regulatory contexts.

In contractile ciliates, centrins acquire an additional, specialized role in mediating calcium-dependent contraction. Previously, ultrastructural studies across multiple contractile ciliates have shown two morphologically distinct types of cortical fiber systems, both of which are thought to contribute to cellular contraction. One system is microtubule based, often associated with classical cytoskeletal functions like support and intracellular transport and the other consisting of fibrils or myonemes, which are thought to mediate rapid contraction in response to calcium influx [20], [21], [30], [31]. These myonemal fibers contain centrin or related centrin-family proteins and are

regulated through calcium binding mechanisms, allowing for ATP independent, high-speed contraction. Centrin binds to Ca^{2}+, undergoing a conformational change which allows cells to contract without ATP hydrolysis [32], [33]. Contraction involves a dramatic change in morphology of the filaments in the myonemes, with the filaments of the myonemes coiling into helical coils during the contraction and becoming thicker and shorter [34], [35]. A related fibrous structure that also contracts in response to changes in Ca^{2+} concentration is the vorticellid spasmoneme [36]. Its principal constituent, spasmin [33], has homology to EF-hand domain proteins such as centrin [37], and is similarly activated by calcium binding. In addition, the spasmoneme also has elastic properties that are not dependent on the Ca^{2+} concentration [36]. Taken together, these systems suggest that centrin containing fibrous assemblies are capable of integrating both active Ca^{2+} triggered contraction and passive elastic recoil. These properties of stimulus driven mechanical response and elasticity may be hallmark features of centrin-based cytoskeletal structures, enabling rapid and efficient cellular movements in ciliates and potentially other mechanosensitive eukaryotic cells.

The assembly of centrin into myonemes with defined orientations relative to the rest of the cell cortex raises the question of what positional information drives their patterned assembly. Centrin-binding partners are likely responsible for the specificity of localization and function of centrin. The founding member of a family of centrin-scaffolding proteins was identified in *Saccharomyces cerevisiae,* where centrin has been shown to have two clear roles in the spindle pole body (SPB): duplication of the SPB and as a constituent of the contractile fibers within and attached to the microtubule-organizing center, which are calcium sensitive [38]. A novel centrin binding protein was

discovered in yeast, which co-localized with the centrin, Cdc31p, at the SPB half-bridge. This protein, Sfi1p, is a 120kDa polypeptide, containing 21 motifs with the consensus sequence $AX_7LLX_3F/LX_2WK/R$, each binding to centrin at a 1:1 molar ratio [38], [39]. Orthologs of this protein Sfi1p, were subsequently identified in many other diverse species.

Within the ciliates, sequence analysis has identified several large centrin-binding proteins containing Sfi1 repeats, suggesting that this family of proteins plays a conserved and functionally diverse role across different species. In *Paramecium tetraurelia*, these proteins have been characterized and shown to be essential for the formation and maintenance of the infraciliary lattice (ICL), a calcium-responsive, contractile meshwork of fibers, containing Sfi1-centrin complexes, that is a prominent component of the *Paramecium* cytoskeleton. The ICL underlies the cell cortex and coordinates with basal bodies and other structural components to support cell shape, contractility, and mechanical stability [40], [41]. In *Tetrahymena*, Sfi1 homologs including sfr1 and sfr13 have been shown to play critical roles in basal body separation, spacing, and cortical organization. These proteins are required for the generation and stability of basal body rows, highlighting the importance of Sfi1-centrin interactions not only in contractile systems but also in templated organelle duplication and spatial patterning of the cell cortex [42], [43]. Supporting this role, Sfi1 repeat proteins have also been identified in *Spirostomum minus*, where they functioning in ultra-fast Ca^{2+} mediated contraction [44], [45]. In *Spirostomum*, the Sfi1 homologs, GSBP1 and GSBP2, are very large in size and assemble into fibrillar scaffolds that contract in

response to calcium signaling, in coordination with their centrin family binding partner, spasmin [44].

In *Stentor*, the contractile fibers, often referred to as myonemes or "M fibers" [5] are described as discrete and prominent bundles in the posterior but linked by extensive side branches in the anterior [5], [20], [21]. These fibers are confirmed to be centrin containing where centrin is largely in the posterior cables of the cell with the fibers narrowing as they approach the anterior end of the cell [22]. At the anterior is a mesh-like network of centrin, creating a continuous sheet around the entire cell [5], presumably to counter the change in internal pressure during rapid contraction where the stalk of the cell contracts to 20-25% of its full extended length [35]. The anterior end of *Stentor*, in contrast, undergoes very little extension or contraction. The frontal field, a region of the cortex at the anterior end of the cell surrounded by the membranellar band, is moderately contractile, but being circular in shape, contracts uniformly in all directions instead of along a single axis [46]. Perpendicular connections to the "M fibers" have been described [2], [20], [47] although it is not yet known whether or not they contain centrin. How does the same centrin protein assemble into such distinct structures in different parts of the cell? Because of the association of Sfi1 family proteins with centrin in other contractile ciliates [40], [42], [44], [45], it is likely that Sfi1 is also involved in cortical fiber systems and contraction in *Stentor*. A prior proteomic analysis of dissected *Stentor* cells indicated that different Sfi1 family members were differentially localized along the anterior-posterior body axis [39]. Could the regionalized patterning difference in centrin into networks versus cables be due to regionalized localization of different Sfi1 proteins?

In order to investigate the interplay of Sfi1 family proteins and centrins in cortical patterning in *Stentor*, we have visualized the centrin based cytoskeleton using expansion microscopy and functionally analyzed a sub-set of Sfi1 proteins encoded by genes that are upregulated during oral regeneration. Our results indicate that the specific Sfi1 isoforms analyzed in this study co-localize with a specific subset of the centrin patterning, suggesting a selective spatial overlap rather than a uniform co-distribution. Furthermore, Sfi1 proteins exhibit distinct organization along the longitudinal axis of the cell, and knockdown of specific Sfi1 members led to altered spatial arrangement of centrin fibers, together pointing to a role in establishing or maintaining regionalized patterning of centrin within the cell cortex. Additionally, we find that Sfi1 proteins may have a functional role in oral regeneration. Specifically, different Sfi1 family members appear to be recruited sequentially to the growing oral primordium, supporting the idea that the primordium scaffold is assembled in a staged manner, with each Sfi1 isoform potentially scaffolding centrin at distinct phases of regeneration. Knockdowns of early expressed Sfi1 genes result in more severe regeneration defects, while late-expressed Sfi1 genes appear to be less essential, possibly due to functional redundancy or their role in later, less critical stages of oral primordium development. Given its role in scaffolding centrin filaments, we also investigated Sfi1 in cellular contraction and observed that some Sfi1 genes play a more prominent role than others. In particular, knockdowns of specific Sfi1 genes led to impaired contractile responses, including either complete failure to contract in response to a stimulus, or a marked reduction in contraction speed. These findings suggest that Sfi1 proteins may have specialized roles in coordinating structural patterning, scaffolding oral primordium growth, and calcium-mediated contractility.

2.3 Results

Regional differences in centrin patterning on the Stentor cortex

Stentor, like other ciliates, has over 100 homologs of centrin and centrin-like proteins. Western blots using the centrin antibody 20H5 show that *Stentor* has centrin and isoforms at the average typical size (20-25kDa) as well as large calmodulins (55-70kDa) and other EF-hands of varying molecular weights **(Figure 2.1B)**. To characterize the plethora of centrin homologs, we first used maximum likelihood to infer a phylogenetic tree with characterized human, yeast, and *Paramecium* centrin and calmodulin sequences as hallmarks. 36 of 80 potential centrin candidates in the *Stentor* genome that were also found in the set of EF-hand proteins identified by proteomic analysis of *Stentor* [9], aligned well to the hallmark sequences common to centrins in other organisms. On our tree, only one sequence (SteCoe_3383) falls into the group of canonical human centrin3-like proteins that are found in most eukaryotes **(Figure 2.1C).** 18 sequences group together with *Paramecium* centrins thought to be ciliate-specific, like the ones found in the infraciliary lattice [48]. 16 sequences fall in the highly diverged group of calmodulin-likes and may not represent bona fide centrin proteins. One sequence (SteCoe_24203) sits in a group sister to centrin3-likes.

To visualize the centrin cytoskeleton, we performed immunofluorescence of centrin using a commercial monoclonal antibody, coupled with expansion microscopy. An expansion factor of approximately 9.2 was calculated from measurements of unexpanded cells and post expanded cells taken from the same culture. Our results show localization in the cortical fibers that run parallel along the cell, particularly in the

posterior, showing dense localization with tapering intensity moving towards the anterior of the cell. In addition to localization in the cortical fibers, the anterior of the cell contains a mesh-like network of centrin with a striking boundary halfway through the cell towards the posterior **(Figure 2.2A).**

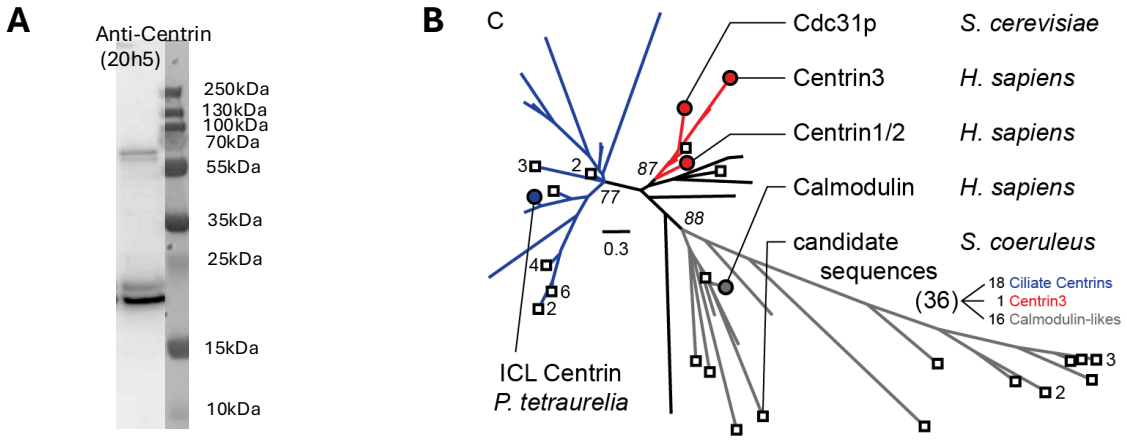

Figure 2.1: Centrin is highly conserved. (A) Western blot of *Stentor* lysates immunoprecipitated with monoclonal anti-centrin (clone 20h5) antibody show bands at estimated centrin sizes (~18-23kDa) and larger calmodulins (55-70kDa). (B) Phylogenetic characterization of *Stentor* candidate centrin sequences. ML tree of 36 *Stentor* sequences (squares) with *Paramecium* and characterized human centrins as hallmarks. ICL, infraciliary lattice. Numbers count sequences at tips. Italic numbers are ultrafast bootstrap support values of 1000 replicates. Branch-lengths represent average amino acid substitutions per site.

When looking at a single z-slice of centrin immunofluorescence using conventional confocal microscopy, ladder-like rungs can be seen in the posterior of the cell, which do

not appear in the maximum intensity projections, which is due to the much greater intensity of the myoneme bundles **(Figure 2.2B)**. This complex pattern raises the question of what is organizing centrin and what makes centrin different in the anterior and posterior? Centrin binding proteins have been shown to have roles in modulating the activity of centrin in different processes such as ciliary and flagellar function and cell cycle regulation[49]. Sfi1, with its many centrin binding repeats and involvement in the myonemal cytoskeleton in other ciliates[44], [45], [50], is a strong candidate for organizing centrin.

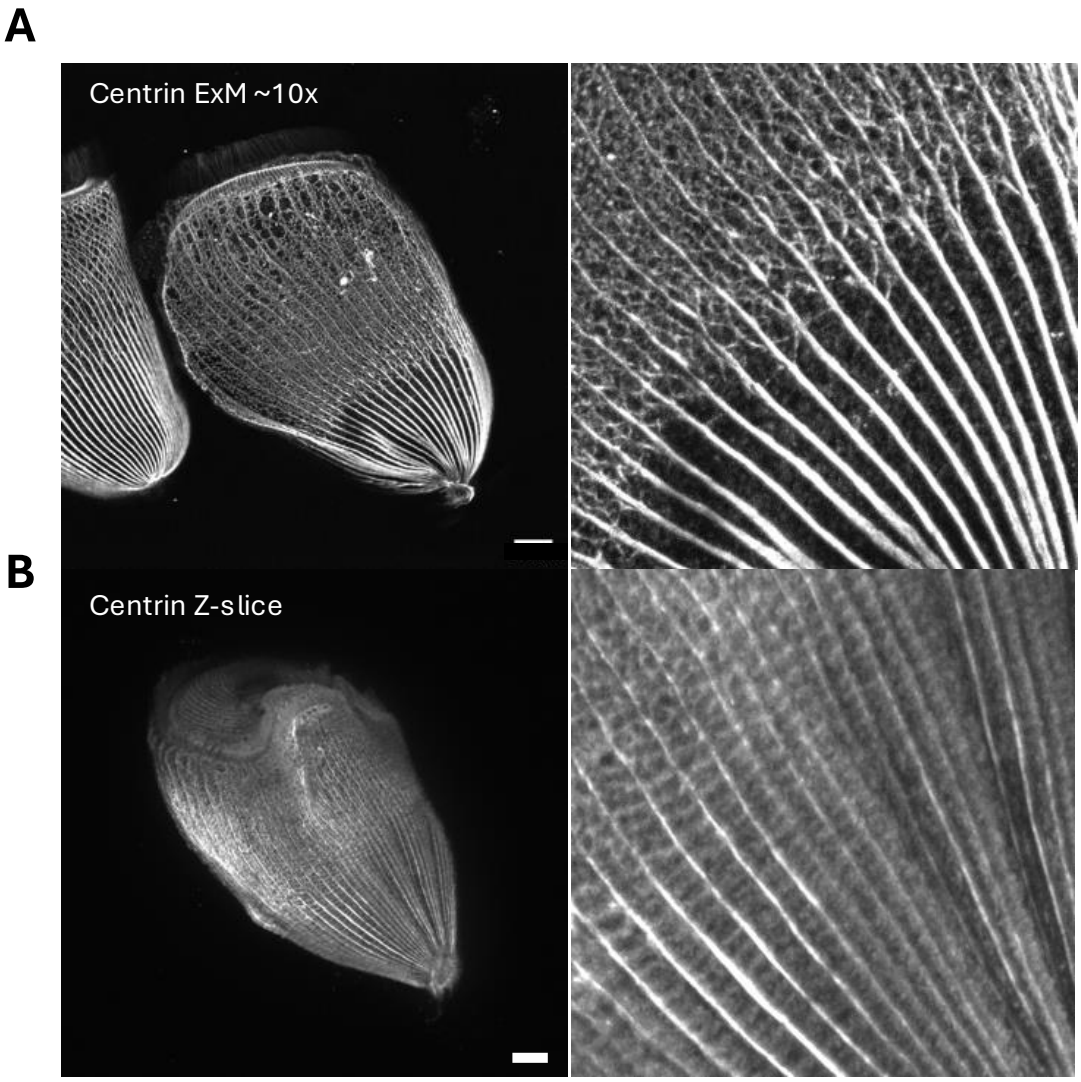

Figure 2.2: Centrin patterning in *Stentor*. (A) Representative example of maximum intensity projection of fluorescence microscopy confocal z-stacks showing *Stentor* centrin immunofluorescence on Magnify expanded cells. Close-up (right panel) highlights the stark change in pattern in the anterior and posterior of the cel and the intricate anterior centrin bundles in between the cortical rows. Scale bar 10um, adjusted for expansion. (B) A single confocal z-slice of centrin immunofluorescence, without expansion. Ladder "rungs" are seen in the posterior between the centrin containing cortical rows that run along the cell.

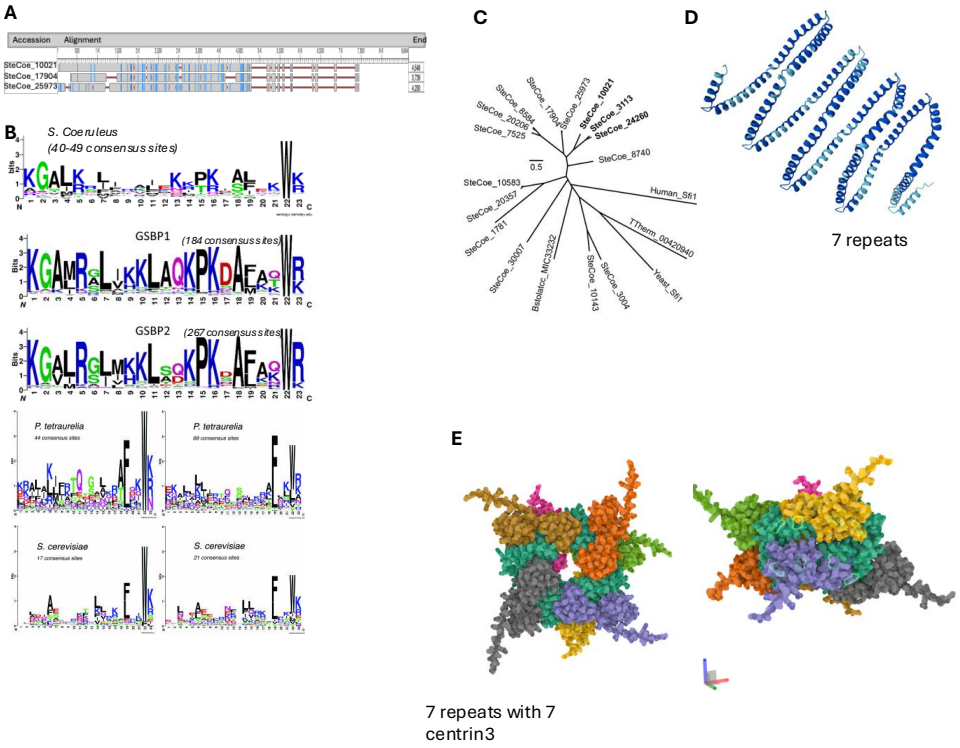

Figure 2.3: Sfi1 in Stentor coeruleus. (A) Blast alignment of three largest Sfi1s in Stentor. (B) Sequence logos of Sfi1 repeats in Stentor, Spirostomum, Paramecium, and Yeast. Stentor sfi1 sequence logo was generated using Sfi1 repeats from SteCoe_17904, SteCoe_25973, and SteCoe_10021 using the tryptophan at the 22nd position as a diagnostic residue. Using relaxed criteria, additional centrin-binding sites (from 44 to 89) were identified in Paramecium. Stentor sequence mostly closely resembles that from S. minus, containing helix-breaking residues alanine and glycine and beginning with KGAL in positions 1-4. (C) Maximum likelihood phylogenetic tree of Stentor Sfi1 homologs showing their relationship to Sfi1 homologs in other organisms including Human, Paramecium (P), Tetrahymena (T) and Blepharisma. (D) Alphafold3 prediction of 7 Sfi1 repeats from SteCoe_17904. Sfi1 repeats are largely alpha-helical, and kink at evenly spaced repeats, creating a coil (E) Alphafold 3 prediction of 7 Sfi1 repeats from (E) bound to 7 centrin3. The centrins, each a different color, bind to the coiled Sfi1 backbone (teal). Diagnostic tryphophans are highlighted (green, right panel).

Stentor contains multiple Sfi1 encoding genes

As with the centrin family, the Sfi1 gene family is also expanded in *Stentor*, with at least 15 members based on motif detection using RADAR and ScanProsite [51], [52]. The largest Sfi1s have high degrees of homology **(Figure 2.3A)**, with up to 49 repeats predicted using a relaxed form of $AX_7LLX_3F/LX_2WK/R$, the canonical motif first discovered in yeast. Compared to the human homolog which contains 23 repeats [38], ciliate Sfi1s have many more repeats, between 2-10 times more [40], [42], [45]. A consensus sequence for the Sfi1 motif was generated in *Stentor* using repeats found in SteCoe_17904, SteCoe_25973, and SteCoe_10021. This consensus sequence in *Stentor* is more similar to those found in other ciliates, in particular *Spirostomum minus*, compared to humans and yeast, as shown by the sequence logos and consistent with the predicted phylogeny. While it still contains the conserved tryptophan at the 22nd position and R/K at the 23rd position **(Figure 2.3B, Figure 2.3C)**, the initial residues appear to be less conserved, with many repeats beginning with a KGAL sequence. The previously reported presence of proline and glycine resides in the sequence signature found in *Spirostomum* [45], which are predicted to create kinks in the alpha-helical structure, are also found in the sequence signature of *Stentor* Sfi1.

Analysis of the Sfi1 sequences revealed a series of internal repeats with the consensus motif separated by gaps of 46 amino acids. This gap is larger than that seen in Sfi1 motifs in humans and yeast. While *S. cerevisiae* Sfi1p repeats vary in length between 23-36 amino acids [39], *Stentor* Sfi1 repeats are more consistently evenly spaced apart. *Stentor* Sfi1 protein structure is predicted to be mainly alpha-helical, as confirmed by an Alphafold3 [53] prediction of seven Sfi1 repeats from SteCoe_17904 **(Figure 2.2D)**.

Because of the large size of the entire Sfi1 proteins and the disordered tails at the N and C terminals, we are unable to predict structures of entire Sfi1 proteins with high confidence. We also used Alphafold3 to predict the structure of these seven Sfi1 repeats bound to seven molecules of centrin 3, which creates a super-helix forming filaments or fibers **(Figure 2.3E)**. Previously, sequence and structural analyses in *S. cerevisiae* show individual centrins stabilized by head-to-tail contacts form a helical filament surrounding the central Sfi1 alpha helix, with spacing between adjacent repeats that varies between 23-33 residues [39]. In contrast, in *Stentor* and *Spirostomum* [45], the organization of centrin-binding regions are highly regular over the majority of the protein's length, containing consecutive 69-amino acid repeats (23 amino acids of the Sfi1 motif plus 46 amino acids before the next motif repeat). In *Stentor*, the centrins are predicted to bind to the core Sfi1 alpha helix, creating a supercoil of alpha-helices, where each turn of the superhelix contains 4 centrin binding sites **(Figure 2.3E)**.

With a large number of Sfi1 family members, we applied two criteria to identify family members most likely to have functions related to spatial patterning. First, we leveraged a strength of *Stentor* in its ability to regenerate patterning after perturbation. To do so, we turned to a transcriptomic analysis of regeneration to identify the candidates most likely to play a role in this process. Multiple Sfi1s are upregulated in various timepoints during the transcriptional program of *Stentor* oral regeneration (**Table 2.1**) [8]. As a second criterion, we leveraged a previous proteomic study to look for Sfi1 family members with significant localization to the anterior of the cell versus the posterior, some Sfi1s are found to be more abundant in the anterior vs the posterior and vice versa

[9], indicating that some, but not all, are more localized to a specific half of the cell and may perform different functions within the cell.

We found that the three largest Sfi1 proteins in the *Stentor* genome, SteCoe_17904, SteCoe_25973 and SteCoe_10021, were all upregulated during oral regeneration, and also showed regionalized enrichment along the anterior-posterior axis, and we therefore selected these three for further analysis. From here on, SteCoe_17904, SteCoe_25973 and SteCoe_10021 will be referred to as Sfi1-1, Sfi1-2, Sfi1-3 respectfully.

To determine the localization of Sfi1 in *Stentor*, we generated separate polyclonal antibodies against each of the three proteins Sfi1-1, Sfi1-2, and Sfi1-3. Because of the high level of homology among the repeats in the three proteins, peptides taken from the N-terminal region, outside the region of the repeated motifs, outside the region of the repeated motifs, were used to generate the antibodies to each of the three proteins.

Table 2.1: Predicted Sfi1 in *Stentor*. Putative Sfi1 with predicted repeats, molecular weight and which cluster (1-5) corresponding to time during regeneration which that particular Sfi1 is upregulated. Half-cell enrichment refers to which half of the cell the Sfi1 protein is more significant in based on proteomic studies.

Accession	Predicted repeats	MW (kDa)	RNAseq cluster	Half-cell enriched
SteCoe_10021	49	495.27	5	Anterior
SteCoe_25973	47	527.27	4	Anterior
SteCoe_17904	40	434.3	2	Anterior
SteCoe_8740	25	239.13		Posterior
SteCoe_17381	24	241.25	2	
SteCoe_3113	23	309.55		Anterior
SteCoe_24260	14	140.78		
SteCoe_20357	13	354.87		
SteCoe_10583	13	360.9		
SteCoe_8584	12	184.41	4	
SteCoe_20206	12	183.51	5	Anterior
SteCoe_7525	10	152.92	3	
SteCoe_30007	7	179.45		Posterior
SteCoe_3004	7	112.07		
SteCoe_10143	4	143.2		

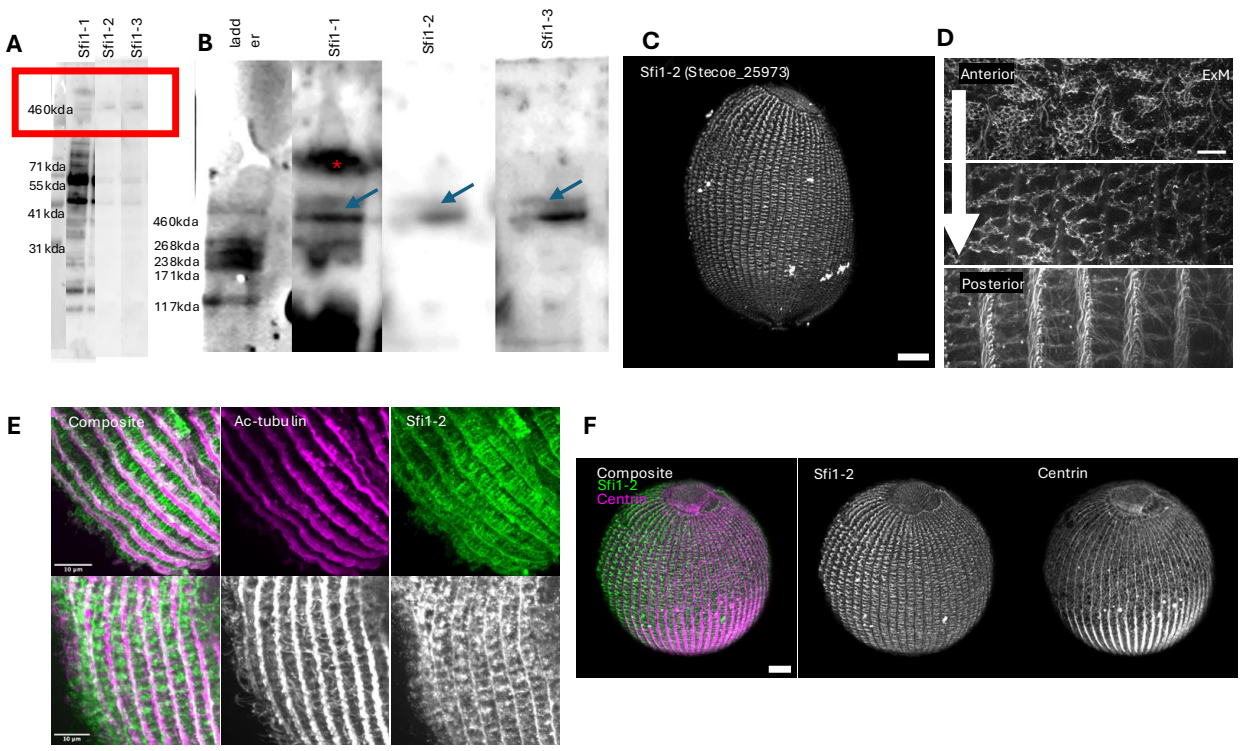

Figure 2.4: Sfi1 localization in *Stentor*. (A) Western blot of custom Sfi1-1, Sfi1-2, and Sfi1-3 antibodies on *Stentor* lysates. Non-specific bands may be *due* to protease activity during lysate preparation, the polyclonal nature of the antibodies, and high homology of Sfi1 proteins. (B) Western blot close-up of high MW area, red asterisk indicates lysate aggregate at the bottom of the well. Large proteins are detected in the estimated size range of *Stentor* Sfi1 (blue arrows) (C) Immunofluorescence images of *Stentor* showing Sfi1-2 localization. Scale bar, 10um (D) Expansion microscopy of Sfi1 anterior mesh (top) gradually moving towards "ladder-rung" bands (bottom) Anterior and middle panels show immunofluorescence with anti-Sfi1-2, bottom panel uses NHS-ester. Scale bar, 1um. (E) Representative images of Sfi1-2 co-labeling with an acetylated tubulin antibody(magenta). The Sfi1 bands do not co-localize with cilia. Scale bar, 10um. (F) Sfi1 and centrin mesh do not colocalize. Pearson's correlation coefficient = 0.42, n=36. Scale bar, 10um.

In Sfi1-2 and Sfi1-3 immunoblots, we see that the antibodies detected large proteins in the expected size range (527.3kDa and 495.7kDa for Sfi1-2 and Sfi1-3 respectively). The Sfi1-1 antibody **(Figure 2.4A),** detected a distinct band at a high molecular weight

consistent with the predicted molecular weight of the Sfi1-1 protein protein (434.3kDa, **Figure 2.4B, arrows**), but also detected a number of significant non-specific protein bands. Additionally, there is staining detected in the aggregated material remaining at the bottom of the loading well **(Fig 2.4B, asterisk)**. Because of the large size of these proteins, they may not all be able to successfully migrate through the gel. Non-specific bands may be due to cross-reactivity because of the high level of homology among Sfi1 proteins or partial degradation of protein due to proteases that may still be present in the cell lysate. To confirm specificity of the antibodies in immunofluorescence experiments, we used a peptide block with corresponding peptides used for antibody production. Antibodies were incubated with their corresponded peptides and immunofluorescence was performed using these pre-incubated antibodies, which led to a virtually complete loss of Sfi1fluorescence intensity per cell for all three antibodies **(Supplementary Figure)**. Immunofluorescence was also eliminated by RNAi knockdown of each of the Sfi1 genes as discussed below **(Supplementary Figure 2.9)**.

Immunofluorescence of all three Sfi1 antibodies showed a similar pattern **(Supplementary Figure 2.10)**, with wide disorganized filaments at the anterior of the cell and more organized, thin, ladder-like rungs in the posterior, as well as tapering cables from the posterior to the anterior **(Figure 2.4C)**. While conventional confocal microscopy reveals different Sfi1 organization in the anterior and posterior of the cell, it is not clear what these differences may be. To take a closer look at the differences between the anterior and posterior, we turn to expansion microscopy to expand our samples by up to 10-fold. Because Sfi1 custom antibodies are not optimized for

expansion microscopy, they produced a very weak fluorescent signal especially in the posterior of expanded cells **(Supplementary Figure 2.11, bottom middle panel)**. In double-labeling experiments we found that several structures stained with Sfi1 antibodies also stained with the general protein stain NHS-ester **(Supplementary Figure 2.11)**. Specifically, the parallel cables that run along the cell, the ladder-like rungs perpendicular to the cables in the posterior, and a banded mesh network in the anterior. The fact that these structures show up with NHS-ester, which labels all protein, suggests that Sfi1 proteins are found within protein-dense structures. We note in particular that the posterior ladder like rungs seen by NHS-ester staining all stain with Sfi1 antibodies. Moreover, within the filamentous network composing these lateral elements, there is perfect co-localization of Sfi1 with NHS fluorescence. Sfi1 antibodies also stain punctate structures outside of the lateral filaments that do not correlate with NHS staining. The high correlation of Sfi1 immunofluorescence and NHS staining within the lateral filaments means that we can image NHS-ester fluorescence to visualize the detailed structure of the Sfi1-containing posterior lateral filaments. A 10x expansion method [54] reveals bands of a mesh network within the anterior bands (**Figure 2.4D, top panel)**, distinct from the centrin mesh-like network in that the mesh is contained within the lateral bands. Each filamentous element composing the mesh measures approximately between 0.73um-2.4um corresponding to 1-4 Sfi1 proteins based on the estimated length of 580nm for an Sfi1 superhelix **(Figure 2.4D)**. Moving posteriorly, the mesh-like filaments become more organized **(Figure 2.4D, middle panel)**, gradually forming a ladder rung organization in the posterior **(Figure 2.4D, bottom panel)**.

The ladder-rung like posterior bands appear to correspond to the connections between M-bands shown in early illustrations of *Stentor* fiber systems [2], [20] in which perpendicular connections connect adjacent longitudinal myonemes. The thickness of the posterior bands spans a length corresponding to several basal bodies in the kinety, such that for every band, there are approximately 2-5 basal body pairs corresponding to 1.7-4um. The lateral bands appear to initiate at the basal bodies, and their length spans the width of the gaps between adjacent myonemes, which corresponds to the pigment stripes **(Figure 2.4D)** ranging from 5-13um depending on the circumferential position of the stripes. The spacing between the bands is not consistent but ranges between 3-9um. The shortest rungs are also the thinnest and increase in thickness with length up to a certain point, after which the thickness can vary. We note that these lateral bands are distinct from cilia as shown by double-labelling with an acetylated tubulin antibody **(Figure 2.4E)**. They lie beneath the cilia, consistent with the z-position of the "M-band connectives" described by Tartar [2]. In contrast with the lack of co-localization of the Sfi1 proteins with centrin in the anterior centrin mesh, in the posterior lateral bands Sfi1 co-localizes with centrin **(Figure 2.2B, Figure 2.4F)** with a Pearson's correlation coefficient of 0.42 determined using the plugin JACoP (https://imagej.net/plugins/jacop) in ImageJ, n=36. Because these Sfi1 co-localize with centrin specifically in the posterior region of the cell, this suggests a region-specific interaction that may reflect functional specialization of the cytoskeletal scaffold along the longitudinal axis, although the possibility that a different Sfi1 co-localizes with the anterior centrin mesh cannot be ruled out.

We conclude that the three Sfi1 proteins selected for this study co-localize with the myonemes and with lateral centrin bands in the posterior part of the cell, but not with the anterior centrin mesh, suggesting they may play a specific role in forming a sub-set of centrin structures.

Role of SFI1 family proteins in maintaining anterior/posterior cortical patterning of centrin

We next tested the functional role of the three Sfi1 family members in cortical patterning of centrin. Cells were microinjected with in vitro transcribed dsRNA directed against each of the Sfi1 family members. Regions of 1.3-1.5kb of each Sfi1 were targeted by RNAi using sequences specific to each Sfi1 (**Supplementary 2.2**). In all three cases, protein depletion was verified by immunofluorescence with the corresponding Sfi1 antibodies. In the case of RNAi mediated knockdown of Sfi1-1 and Sfi1-2, cells stained with anti-centrin antibodies revealed the loss of the distinct anterior and posterior differences in centrin patterning. In both cases, the mesh-like network normally seen only in the anterior of control cells now appears in both the anterior and the posterior, while the thick myonemes normally seen in the posterior show notably reduced centrin incorporation **(Figure 2.5A)**. In Sfi1-3 RNAi cells, centrin retains its distinct anterior/posterior patterning. We quantified this observation by measuring the textures of the anterior and posterior across 3 points in each cell using the GLCM texture analyzer in ImageJ and took the ratio of the posterior over the anterior, where a greater ratio indicates more distinct textures **(Figure 2.5C)**. In addition to the loss of posterior

structures in the Sfi1-1 and Sfi1-2 RNAi cells, we also found that the mesh-like network in the anterior is much less dense and appears disassembled or disrupted compared to control cells **(Figure 2.5B)**. Thus, both the anterior and posterior halves of the cell show abnormalities in centrin distribution, with the main phenotype being a reduction in the regional differences in patterning between the two halves. The overall integrated fluorescence intensity of centrin immunofluorescence staining is not significantly different in the RNAi cells compared to controls, showing that the distribution is altered but not its overall abundance **(Figure 2.5D)**. The fact that the overall centrin fluorescence is not affected in RNAi knockdowns is consistent with distinct Sfi1 isoforms playing site-specific roles in patterning rather than globally affecting centrin gene expression or protein stability.

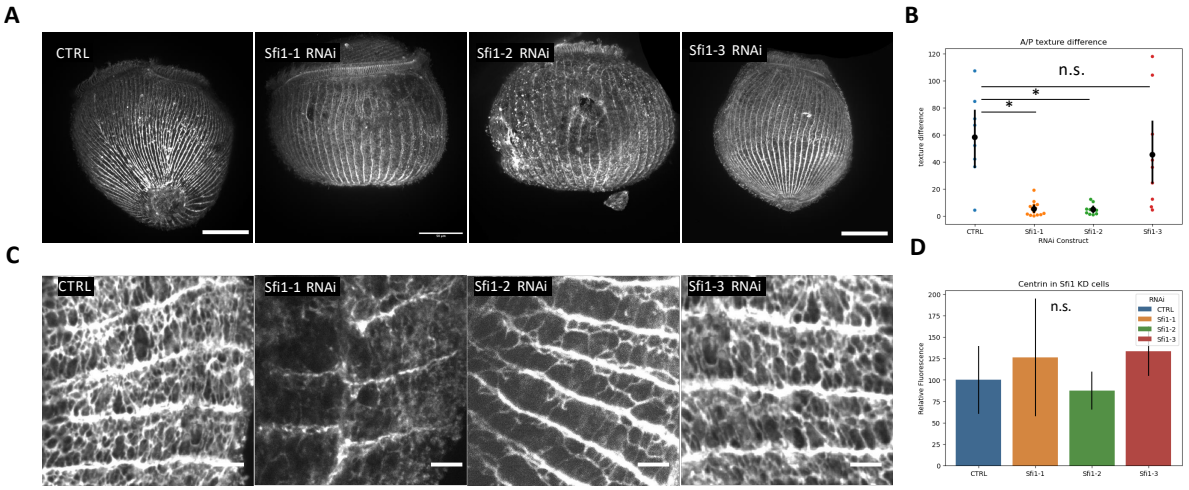

Figure 2.5: Centrin patterning in Sfi1 knockdown. (A)Immunofluorescence of centrin in Sfi1 RNAi knockdowns. Scale bar 50um, statistical significance measured using t-test. (B) Immunofluorescence imaging of centrin in the anterior of *Stentor*. Much of the dense, mesh-like structures are disassembled in the Sfi1-1 and Sfi1-2 knockdowns. Scale bar 1um. (C) Plot showing anterior/posterior texture difference. (Figure caption continued on next page.)

(Figure caption continued from previous page.) Three sections of the anterior and three sections of the posterior of each cell was texture analyzed using a GLCM texture analysis. The average ratio of the posterior over the anterior was calculated for each condition. A lower texture difference indicates that the anterior and posterior textures are more similar. The average texture differences are 58.3 for CTRL n=9, 5.3 for Sfi1-1 n=14, 4.9 for Sfi1-2 n =11, and 45.4 for Sfi1-3 n=11. Statistical significance was calculated using a student's two-tailed t-test where $p<0.5$ (D) Plot showing the Corrected Total Cell Fluorescence of cells (n=10) stained with centrin. The total fluorescence intensity is not significant between the Sfi1 knockdowns and the control.

Sfi1 proteins required for progression of oral regeneration

Classically, *Stentor* has been used as a model for regeneration, due to its amenability to microsurgical manipulations, and robust regeneration assays [2]. When exposed to a sucrose shock or bisected with a glass needle, *Stentor* will regenerate a new oral apparatus over the course of 8-10 hours at room temperature. Oral regeneration begins with assembly of basal bodies and associated structures at the oral primordium site, where the narrow and wide cortical cables intersect. This precise location on the ventral surface of the cell is at a considerable distance from the position of the original oral apparatus. The basal bodies eventually form an oral primordium which elongates along the cell, curls upward at the posterior end to form a new buccal cavity or gullet, and finally migrates to the anterior of the cell to the normal position occupied by the membranellar band **(Figure 1.2)**. While previous studies have produced a transcriptional profile of regeneration and a proteomic analysis [8], [9], [11], [55], much less is known about specific molecular players controlling this complex morphological process. Microsurgical experiments have shown that the signal for the initiation of regeneration travels over the cortex [56]. Local anesthetic such as tetracaine and dibucaine which act on the cell membrane and affect calcium metabolism have been

shown to delay oral regeneration, specifically in early stages when much of the primordium is being built [57]. This delay might then be caused by the disruption of cytoskeletal elements involved in transmitting the stimulus for oral primordium formation. Given that oral regeneration involves formation and alignment of thousands of basal bodies and requires a signal that travels through the cytoskeleton and that might involve calcium binding proteins, we reasoned that centrin and Sfi1 proteins might play a role in regeneration.

The three Sfi1 proteins analyzed in this study were all encoded by genes showing upregulation during oral regeneration [8]. However, their timing of expression was different. Our previous transcriptomic analysis indicated five distinct clusters of gene expression based on the timing of peak expression. The earliest expressed cluster was designated cluster 2, with clusters 3-5 peaking at progressively later times during regeneration. Sfi1-1 is upregulated early in regeneration, in cluster 2, which is also the time of peak expression of centriole biogenesis related genes and corresponds to the time when new basal bodies, that will ultimately assemble into the membranellar band, first start to appear. Sfi1-2 peaks several hours later in cluster 4, which corresponds to the time at which motile cilia have assembled onto the basal bodies and the cilia have begun to align into the structure of the membranellar band. Sfi1-3 peaks later in regeneration in cluster 5, the time when the oral primordium has fully assembled and the cell is now re-organizing its microtubule fibers anterior of the oral primordium to place it at the anterior end of the cell.

To test the role of Sfi1 family members in regeneration, each of the three Sfi1 genes were knocked down by RNAi and then the cells were induced to regenerate using a sucrose

shock which removes the oral apparatus **(Figure 2.6A)**. RNAi was confirmed to result in reduction in protein quantity, using quantification of Sfi1 intensity in immunofluorescence images **(Supplementary Figure 2.10)**. The Sfi1-1 and Sfi1-2 RNAi cells started to regenerate, forming a membranellar band, but did not fully regenerate and remained in stages 4-6, such that the oral primordium formed but did not complete migration to the anterior of the cell **(Figure 2.6B, Figure 2.6C)**. Additional timepoints at 24 hours post shock (data not shown) were taken to confirm that regeneration would not continue beyond the typical 8-hour time period. In Sfi1-3 RNAi cells, however, the cell is able to completely regenerate forming a fully normal looking membranellar band at the anterior of the cell. These findings suggest that the earlier expressed isoforms, Sfi1-1 and Sfi1-2, are required for the later stages of regeneration which includes the elongation and migration of the oral primordium along the cell.

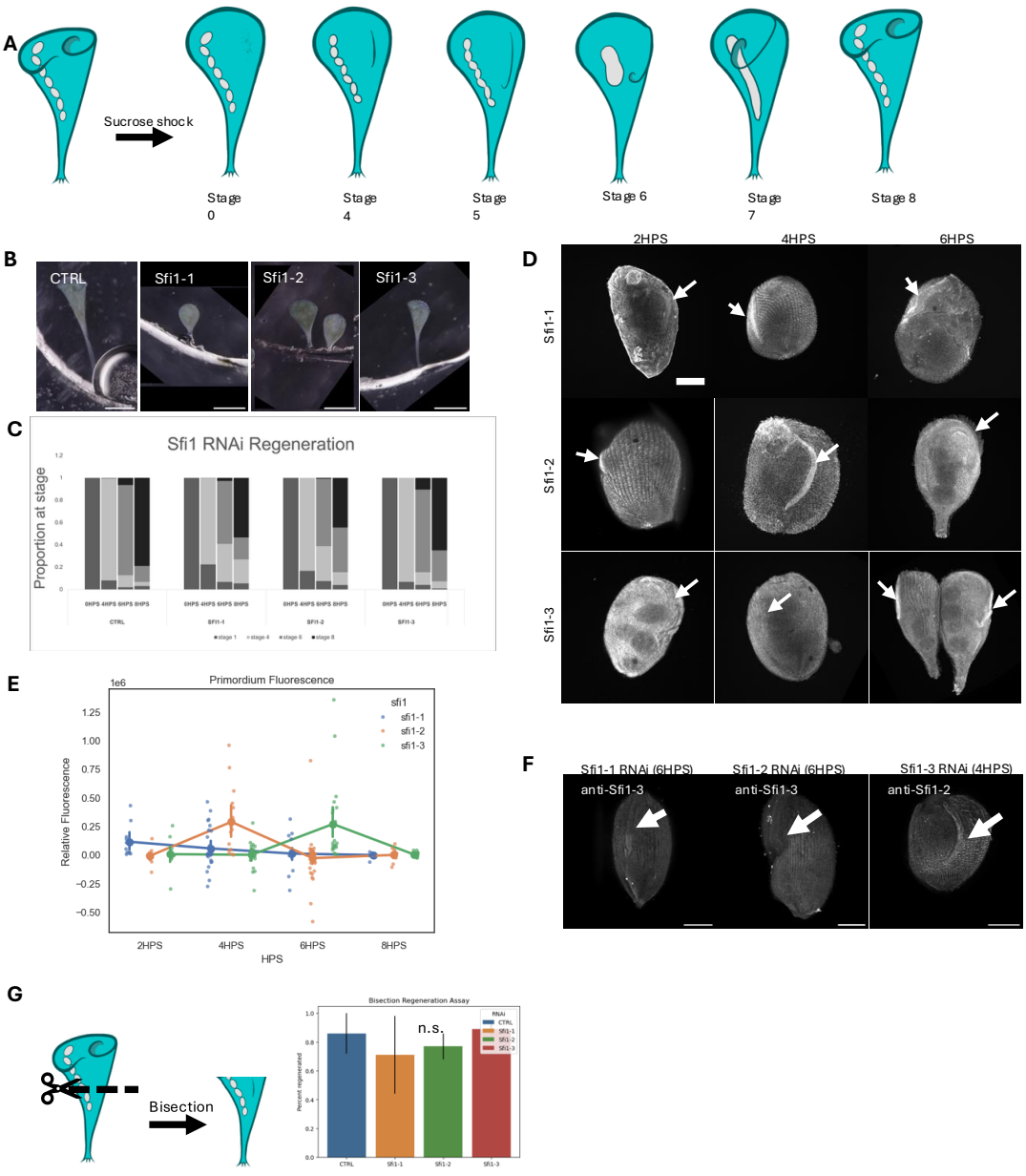

Figure 2.6: Sfi1 plays a role in *Stentor* regeneration. (A)Regeneration assay in *Stentor*. Each stage corresponds to hours post sucrose shock. Sucrose shock is used to induce shedding of the membranellar band. Once removed, the cell regenerates a new oral apparatus, first with basal bodies assembling at the primordium site. The primordium elongates along the length of the cell (Stage 4) and curves at the posterior end to form the gullet (Stage 6). (Figure caption continued on next page.)

(Figure caption continued from previous page.) This structure then migrates to the anterior of the cell to the position of the original oral apparatus (Stage 8) by 8HPS. Membranellar bands are visible at the anterior of the control and Sfi1-3 RNAi cell, having a conical shape. Sfi1-1 and Sfi1-2 RNAi cells are missing the ring of cilia at the anterior, creating a rounded, tear-drop shape. Scale bar 100um. (C) Plot showing the percent of cells that have reached the corresponding stage of regeneration at that timepoint. A larger proportion of Sfi1-1 and Sfi1-2 RNAi cells remain in stages 4-6 compared to control and Sfi1-3 RNAi cells. Data was generated from 5 independent trials, each with n=20-120. (D) Representative images of maximum intensity projection of confocal z-stacks showing a time course of oral primordium growth during regeneration with immunofluorescence of corresponding Sfi1 antibodies. Arrows indicate the oral primordium. Scale bar 50um. (E) Plot depicting corrected total fluorescence of Sfi1 in the oral primordium at different timepoints. Sfi1-1 intensity peaks early in regeneration (2HPS) and gradually decreases. Sfi1-2 peaks at 4HPS, and fluorescent is largely absent from the oral primordium at 6HPS, as seen in (D). In contrast, Sfi1-3 has fluorescence visible in the primordium only at 6HPS, although the fluorescence of the whole cell across timepoints remains relatively constant. Bars indicate mean fluorescence intensity. Sfi1-1 n=14, 17, 27, 18; Sfi1-2 n=33, 25, 35, 20; Sfi1-3 n=20, 16, 38, 31 for each respective timepoint. (F) Representative images of early and mid (left and middle) Sfi1 RNAi cells stained with Sfi1-3, showing no localization to the oral primordium, and IF of Sfi1-2 in Sfi1-3 knockdown (right) showing some localization. (G) Plot showing percent of Sfi1 RNAi cells and controls that completed regeneration in 8 hours post bisection with a glass needle. Bars indicate mean proportion of cells that regenerated, and lines indicate S.E.M. with control 0.86±0.14, Sfi1-1 0.71±0.27, Sfi1-2 0.77±0.09 and Sfi1-3 0.89±0.02. Three independent trials were performed, each with n=20-35 cells. The percent regenerated across all conditions is not statistically significant, as calculated using a student's t-test with $p>0.05$.

Time course analysis of Sfi1 localization to the oral primordium during regeneration revealed distinct temporal patterns for each isoform. Sfi1-1 fluorescence in the oral primordium peaks at early timepoints, in this case at 2 hours post-shock (HPS) **(Figure 2.6E)**, which roughly coincides with the period of Sfi1-1 gene expression[8]. Once the oral primordium becomes visible, usually at 4HPS, Sfi1-1 is seen in the primordium **(Figure 2.6D, arrow)** as shown by the increase in immunofluorescence. However, by 6HPS much of that intensity is lost. In the case of Sfi1-2, fluorescence in the oral primordium peaks at 4HPS and with clear localization in the oral primordium and

similarly shows reduced signal at 6HPS. In contrast, Sfi1-3, **(Figure 2.6D, E)** shows maximum recruitment to the primordium at 6HPS but not 4HPS **(Figure 2.6D)**. These data suggests that these Sfi1 proteins are sequentially recruited to the primordium, with timing consistent with their transcript expression during regeneration. We propose a model where a sequential deployment of distinct scaffolds occurs, much like passing a baton in a relay race where each runner is dependent on the previous runner. This sequential localization pattern supports the idea that Sfi1 isoforms are differentially and temporally regulated. We next asked if earlier scaffolding Sfi1 are required for the recruitment of later expressed Sfi1. When we look at Sfi1-3 immunofluorescence in Sfi1-1 and Sfi1-2 knockdown cells, we see an absence of signal in the oral primordium **(Figure 2.6F)**. However, if we look at the Sfi1-2 intensity in Sfi1-3 RNAi knockdown, we do see signal in the oral primordium **(Figure 2.6F, right panel)**. These data suggest that not only are different Sfi1 isoforms sequentially localized to the oral primordium, but their recruitment requires prior recruitment of earlier Sfi1 isoforms to the regenerating oral primordium, indicating a sequential scaffolding mechanism.

Time course images also revealed a loss and re-establishment of Sfi1 bands during regeneration. In the first 3 hours of regeneration **(Supplementary Figure 2.12)**, the lateral bands become more punctate until eventually fluorescence occurs only in the longitudinal cables. The punctate bands re-appear and eventually resume their normal appearance near the end of regeneration. We speculate that this changing pattern of Sfi1 protein localization could be due to a temporary shift of Sfi1 from the ladder rung-like bands of the cytoskeleton to the oral primordium during regeneration.

The foregoing analysis was based on inducing oral regeneration by sucrose shock, which causes the cell to shed its existing oral apparatus including the membranellar band, although it retains the frontal field (region of the anterior bounded by the membranellar band). When *Stentor* cells are bisected with a glass needle, the anterior half-cell retains the membranellar band, but the posterior half-cell has to regenerate a new one. Interestingly, Sfi1 RNAi cells triggered to regenerate using bisection with a needle, rather than with sucrose shock were fully able to complete all stages of regeneration of the oral apparatus **(Figure 2.6G)**. This is consistent with the fact that Sfi1 transcripts are upregulated in the sucrose shock response to regeneration but not the bisection response [8]. Potential differences between the two regeneration paradigms include the fact that the frontal field is removed in bisection but not in sucrose shock, or that the bisected cell will make a much smaller oral apparatus, proportional to its new body size [6], reducing the need for basal body biogenesis. In any case, the fact that RNAi of Sfi1 family members expressed during regeneration in sucrose shock but not bisected cells, has an effect on the process in the former but not the latter case, further supports the specificity of the RNAi phenotypes observed.

Role of Sfi1 in cellular contractile machinery

We have shown that Sfi1 isoforms play a role in patterning centrin on the cell cortex. This cortical centrin patterning is visually striking and structured, but does it have any physiological function? One possibility is that this centrin organization contributes to the mechanical properties of the cell, such as its contractility. *Stentor* is capable of contracting from an extended trumpet shape to a compact sphere on a scale of milliseconds **(Figure 2.7A)**. This dramatic reduction in total body length is driven by specialized contractile fibers known as myonemes. These myonemes undergo a dramatic change in morphology of the filaments upon stimulation by intracellular calcium influx, coiling into helical structures [34], [35]. The myonemes rapidly shorten in length and thicken in diameter. When relaxed, the myonemal filaments have a diameter of 40Å, but once contracted the diameter is increased to 120Å [46]. When contracted, the bundles of microfilaments that make up the myonemes are straight, but when the cell is extended, they become sinuous folds [5]. This transition enables both force generation and spatial reconfiguration of the cell body.

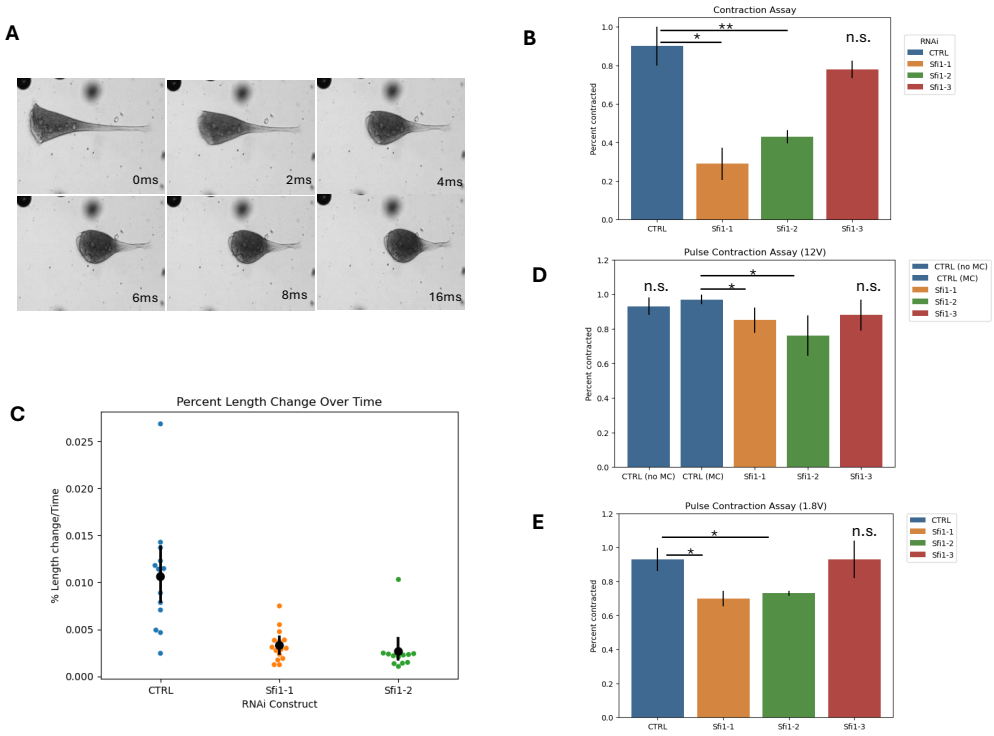

Figure 2.7: Role of Sfi1 in contractile machinery. (A) Representative still frame images of a contracting *Stentor* cell. Contraction occurs over timescale of milliseconds. (B) Plot showing the percent of cells that contract in response to the mechanical stimulus of being pipette up with a P20 pipette. Data was collected over 3 independent trials, with n=50 for each condition. *p<0.05, **p<0.005 (Sfi1-1, p=0.0015, Sfi1-2 p=0.00026, Sfi1-3 p=0.11). (C) Plot showing the percent of length change over time ratio for each condition. The average percent of length change over time for control cells is 0.82±0.59% per millisecond. For Sfi1-1, the average is 0.27±0.17% and for Sfi1-2, 0.20±0.04% per millisecond. (D) Plot showing the percent of cells that contract in response to a constant pulse of 12V. No statistical significance between control cells in spring water (CTRL no MC) and controls in 1.5% methylcellulose (CTRL mc, p=0.26). Sfi1-1 and Sfi1-2 show a decrease in contractility as compared to controls in methylcellulose. *p<0.005 (Sfi1-1 p=0.005, Sfi1-2 p=0.006). (E) Plot showing the percent of cells that contract in response to a constant pulse of 1.8V. Sfi1-1 and Sfi1-2 show a decrease in contractility as compared to controls in methylcellulose (Sfi1-1 p<0.005, Sfi1-2 p<0.5).

Given that centrin has established roles in other ciliate contractile systems [40], [44], [45], [50], [58], it is possible that the patterned organization of centrin could serve to modulate myoneme activity, ensuring that contraction occurs in a coordinated manner across the large surface of the cell.

To test the role of Sfi1 in contraction, we knocked down Sfi1 using RNAi and stimulated contraction by pipetting extended cells into a P20 pipette tip. In four trials each with n~50, 86.7%±4.5 of control cells contracted in response to the pipetting stimuli. Sfi1-1 knockdown cells, (24.3%±8.4) and Sfi1-2 knockdown cells (46.3%±3.4) responded to the stimulus much less than the controls. 72%±10.4 of Sfi1-3 knockdown cells contracted, showing a less severe contraction phenotype **(Figure 2.7B)**. These results indicated that Sfi1 RNAi cells are still able to contract but did not indicate whether they contract at the same speed as controls.

Because *Stentor* contract on a scale of milliseconds, we turn to high-speed imaging at 5000 frames per second. Cells were gently flattened and allowed to extend on a 9mm spacer on a glass slide and contraction was stimulated with a mechanical force in the form of a gentle tap on the slide. Percent changes in cell length were not statistically significant between controls (n=14, 45.1±7.6) and Sfi1-1 (n=15, 41.1±7.8), however, some Sfi1-2 knockdowns (n=13, 35.9±2.9) do not contract as dramatically. Rather than contracting into almost perfect spheres, they contract to a longer, teardrop shape. Upon further analysis, the most dramatic effect was on the amount of time between contraction initiation and termination, which increased in both Sfi1-1 and Sfi1-2 knockdowns. On average, control cells completed contraction in 55.5±35.6 milliseconds, whereas Sfi1-1 and Sfi1-2 knockdowns completed contraction in 152.44±69.9 and

180.1±72.65 milliseconds respectively. Thus, contraction speed is much less in these knockdowns compared to control cells **(Figure 2.7C)**.

To confirm that these results are not dependent on inconsistencies in pipetting or mechanical stimuli, we repeated the analysis using electrical pulses, which can also stimulate contraction in *Stentor*[46]. *Stentor* cells were placed in 1.5% methylcellulose and in a spacer made from flat pieces of steel functioning as electrodes with a gap of approximately 18-20mm. A coverslip was placed on top and using a short pulse of 12V, cells were stimulated to contract. Images pre and post stimulus were taken and percent of cells contracted calculated for each experiment. Cellular contraction was not significantly affected in methylcellulose (n=30-39 over 4 trials, percent of cells contracted 96.8±2.7) as compared to contraction in spring water (n=16-31, 4 trials, 93.0±5.3. While the results are not as dramatic as the previously described assays, Sfi1-1 (n=20-50, 6 trials, 84.7±7.3) and Sfi1-2 (n=20-28, 6 trials, 76.5±11.7) knockdowns show a statistically significant reduction in number of cells that do not immediately contract after an electrical stimulus **(Figure 2.7D)**. Consistent with previous assays, Sfi1-3 (n=23-43, 6 trials, 87.8±9.4) knockdowns contract at a rate within the range of control cells. We note that some of the cells contracted, but after a delay. To see if this occurred more often in Sfi1 knockdown cells, we repeated this experiment with a much lower pulse of 1.8V. While there was no significant proportion of delayed contracting cells, the lower force showed a stronger phenotype in Sfi1-1 (n=16-29, 4 trials, 70.3±4.5) and Sfi1-2 (n=10-21, 4 trials, 72.6±1.4) compared to controls (n=15-29, 3 trials, 93.2±6.9) and Sfi1-3 (n=12-34, 4 trials, 93.0±1.2) **(Figure 2.7E)**. These results indicate that proper Sfi1 function is required for the rapid contraction mechanism in *Stentor*. Loss of Sfi1

disrupts centrin organization, which correlates with impaired contraction, where contraction is either incomplete or does not occur in response to a stimulus.

2.4 Discussion

Regionalized patterning by regionalized distribution of scaffolding proteins

Regionalized differences in protein localization may occur through various processes such as membrane trafficking, cytoskeletal organization, localized translation, signaling pathways, and post-translational modifications. These processes are coordinated to work together to establish and maintain localized expression of proteins. For instance, in neurons, AnkryinG is essential for organizing ion channels in the axon initial segment, the compartment that initiates action potentials and maintains neuronal polarity [59]. The localized accumulation of AnkryinG serves as a cue for the recruitment and assembly of complex molecular machinery in a site-specific manner. Without AnkryinG, maintenance of the axon initial segment is lost, along with neuronal polarity [60]. In the case of Sfi1 and centrin in *Stentor*, one compelling possibility could be that Sfi1 acts as a spatially organized scaffolding protein that governs the subcellular localization and assembly of centrin complexes. Scaffolding proteins are known to serve as molecular organizers, bringing together specific binding partners in defined cellular regions to enable the formation of higher-order structures or signal transduction networks. In this context, Sfi1 may play a critical role in anchoring centrin molecules along the contractile cytoskeleton in a manner that is not uniform but rather regionally

patterned across the anterior-posterior axis of the cell. By compartmentalizing centrin assembly through a polarized and temporally varying distribution of distinct Sfi1 scaffolds, the cell can exert spatiotemporal control over cytoskeletal assembly, enabling the development of functionally distinct cellular domains. Thus, the Sfi1 scaffold may not only provide structural support for centrin binding, but it may also serve as a developmental or functional organizer, encoding spatial information into the architecture of the contractile cytoskeleton. This interpretation is further supported by the observation that the disruption of Sfi1 leads to decreased centrin mesh density and integrity of centrin-based cytoskeletal structures.

The model in which regional differences in the spatial arrangement of centrin fibers are produced by regional differences in Sfi1 isoform composition, is appealing because it reduced a very difficult problem (how to generate different complex 3D arrangements of filaments) into a simpler problem (how to generate differences in abundance of different proteins). Essentially, this model invokes patterning at the level of a scalar variable (Sfi1 abundance) to explain patterning at the level of a higher dimensional function (organization of centrin into different types of filament-based structures).

We note that, in addition to its well-characterized centrin binding repeats, Sfi1 also contains numerous putative calmodulin (CaM) binding sites, suggesting a potentially broader regulatory role in the assembly or modulation of the cytoskeleton. Calmodulin is a highly conserved calcium sensor and signaling adaptor and can act as a protein linker and regulator of scaffold proteins [61]. It can also bridge between different domains on same protein or can physically link two identical or different target proteins together. Structurally, CaM is made up of two independently folded lobes with the

capacity of binding two Ca^{2+} ions each. The two lobes are made up of a pair of EF-hands each and they are connected by a long and flexible linker region, allowing the molecule to adopt diverse conformations in response to calcium signaling. The presence of predicted CaM-binding sites in Sfi1 raises the possibility that Sfi1 may serve as a multi-valent scaffold, coordinating interactions not only with centrin but also with calmodulin in a calcium-dependent manner. This dual interaction potential could enable Sfi1 to integrate mechanical and calcium-signaling cues, modulating its structural or organizational role within the cytoskeleton. For instance, calmodulin might regulate the binding affinity or conformation of Sfi1-centrin complexes, or alternatively, act as a dynamic crosslinker between Sfi1 filaments or adjacent cytoskeletal structures. Supporting this hypothesis, previous studies using calmodulin antagonists, trifluoperazine and W-7, have been shown to delay oral regeneration in *Stentor* [62], suggesting that calmodulin is involved in the control or formation of the oral apparatus. It could be possible that calmodulin is involved in scaffold remodeling or reorganization during regeneration. Preliminary immunofluorescence imaging using an anti-calmodulin antibody further reveals a subcellular distribution pattern similar to that of Sfi1, reinforcing the idea that these two proteins may colocalize or interact with each other. While these observations are suggestive, direct biochemical or structural evidence for a Sfi1-calmodulin interaction has not been determined. Given the similarities between CaM and centrin, it could also be possible that CaM antagonists can bind to centrin itself, as previously shown in *Euplotes* [63]. Additional experiments, such as co-immunoprecipitation, in vitro binding assays, or cryo-EM structural analysis, will be needed to determine whether calmodulin binds directly to Sfi1 or whether such binding induces calcium-dependent conformational changes in the Sfi1 scaffold. Establishing

this interaction would provide a mechanistic link between calcium signaling and contractile cytoskeletal organization, further supporting the role of Sfi1 as an integrative scaffold in the functional polarization of *Stentor* cells.

Comparison with other cell types

Prior work on Sfi1 has established its role as a conserved component of the contractile cytoskeleton across multiple ciliates. In *Paramecium*, Sfi1 has been identified as a structural component of the ciliary lattice, a cortical scaffold that supports the coordinated beating of cilia and likely contributes to maintaining cortical architecture [40]. Similarly, in *Spirostomum* it is involved in the contractile cytoskeleton, which drives its rapid and forceful contractions [44], [45]. Additionally, in *Vorticella,* Sfi1 localizes to the spasmoneme, a contractile stalk that rapidly coils like a spring in response to stimuli [50]. These findings underscore a broadly conserved role for Sfi1 in contractile systems among ciliates, in coordination with centrin and related proteins. Here, we extend these observations by demonstrating that Sfi1 in *Stentor coeruleus* is also a component of the contractile cytoskeleton, but with a more complex and multifunctional role. In addition to supporting contractility, our data shows that Sfi1 is sequentially recruited to the oral primordium during regeneration, where it may function as a scaffold for oral primordium growth.

The centrin-Sfi1 complex appears to be conserved throughout many eukaryotes, and our findings support this for *Stentor*. The repeated motif characteristic of Sfi1 proteins contains the conserved tryptophan at the 22nd residue, with each repeat binding to one

centrin molecule. The predicted structure contains long alpha-helices arranged in a coiled-coiled structure. *Stentor,* like other ciliates, has more centrin binding repeats compared to humans and yeast. In yeast, Sfi1 localizes to the spindle pole body where it forms long filaments with Cdc31 and serves as a scaffold for spindle pole body duplication. C-terminal domains interact with other Sfi1 molecules, allowing for anti-parallel dimerization [38].

Evidence in ciliates shows that Sfi1 and centrin complexes link together to form a dense, fishnet-like mesh [40], [44], [45]. The *Paramecium* Sfi1 ortholog, PtCenBP1 is of similar size and structure as *Stentor* Sfi1, where the PtCenBP1gene encoding a 3.8k -aa protein with a theoretical molecular mass of 460kDa of largely alpha-helical structure with coiled-coiled arrangements and the N and C termini, consistent with a filamentous protein able to form homopolymers [40]. The dem1 mutant, which contains a truncated Pt*CenBP1* is characterized by having sparse ICL meshes and decreased branching [40], much like what we observe in *Stentor*, Sfi1-1 and Sfi1-2 knockdowns.

Spirostomum minus Sfi1 orthologs GSBP1 and GSBP2 are much larger (1458kDa and 2008 kDa) and contain 184 and 267 Sfi1 repeats [44]. These large proteins, along with its centrin family binding partner spasmin, are able to form protein complexes that resemble ropes that are part of a contractile mesh-like fibrillar system. This mesh is organized as numerous parallelograms, much like the *Paramecium* ICL. The parallelograms shrink in the cell's contracted state, causing the fibrillar bundles to shorten and thicken [44]. In contrast to such regular geometric arrangements, *Stentor* Sfi1 anterior mesh appears with an irregular, banded appearance. Studies have shown that myoneme bundles in *Stentor* do shorten and thicken with contraction [5], [46],

however, we have not been able to observe the difference in the mesh in immunofluorescence of extended and contracted cells due to rapid contraction of cells upon fixation. In *Spirostomum minus*, contractility was tested using different extracellular Ca^{2+} concentrations, which induces spontaneous contraction of the cell. With increasing Ca^{2+} concentration, the average time required for cell contraction reduced. In RNAi experiments, it was observed that some RNAi cells did not contract even in elevated, suggesting that structural integrity of the contractile myoneme mesh is essential for calcium-induced contractility. Indeed, disruption of the mesh-like scaffold could be observed in these non-contractile cells. These results closely mirror our findings in *Stentor*, although increasing extracellular Ca^{2+} did not result in spontaneous contraction, and thus other external stimuli were used in our experiments to induce contraction, ensuring that the failure to contract in knockdown cells was not due to insufficient signaling input but rather to defects in the contractile machinery itself.

The greatest difference in *Stentor* Sfi1-centrin scaffolds from these other ciliate systems are the polarized regional differences. This may be due to the contrast in cell shapes. *Spirostomum* adopts a long, cylindrical shape that is tapered on both ends and *Paramecium* are ovoid with a rounded anterior and slightly pointed posterior. These cells contract along their entire body axis, and the geometric mesh of the contractile centrin cytoskeleton in these ciliates is largely uniform across the cell bodies. In contrast, *Stentor* cells are trumpet-shaped, with a flared anterior and a stalk-like tail at its posterior. Although this shape may bear greater resemblance to another contractile ciliate *Vorticella*, the stalk of *Vorticella*, containing the highly contractile spasmoneme, is a separate structure from the zooid or cell body, and contracts like a spring. In

Stentor, the entire cell contracts, with its posterior being more contractile than its anterior. Another ciliate with a highly polarized cell shape is *Lacrymaria*, a teardrop shaped predatory ciliate with a highly contractile neck. Like *Stentor*, its centrin cytoskeleton has differences in anterior-posterior patterning [22], [58]. In the contractile neck of *Lacrymaria*, centrin forms strand-like fibers, whereas in the cell body, it is distributed in a network. However, in a proteomic analysis, Sfi1 homologs are not found in the *Lacrymari*a [58]. Contraction in this system, likely involves an actin-myosin system [58]. While the Sfi1-centrin complex is a broadly conserved feature of contractile cytoskeletons across ciliates, its structural organization and functional deployment are uniquely adapted to each organism's cell shape, contractile demands, and spatial patterning, with *Stentor* exhibiting particularly polarized and specialized architecture.

Sequential scaffolding

Our data suggest that Sfi1 proteins are recruited to the oral primordium in a defined temporal order, supporting the model that the scaffold required for primordium growth is assembled sequentially. Among these, Sfi1-3 appears to be recruited in later stages of regeneration, and its knockdown correspondingly results in minimal or negligible defects in regeneration. This suggests that Sfi1-3 may not be essential for early stages of scaffold formation or that functional redundancy among Sfi1 isoforms allows other Sfi1 proteins to compensate for its absence. In contrast, Sfi1-1 and Sfi1-2, which are expressed earlier during regeneration, may play more central roles in establishing the

structural framework of the developing primordium. Their knockdowns lead to more severe phenotypes, implying that the early scaffolds they form are more critical to initiate and sustain proper morphogenesis.

We propose a model in which Sfi1 isoforms operate in a relay-like sequence, with each variant scaffolding centrin assemblies at specific developmental timepoints. For example, Sfi1-1 may scaffold centrin in the early primordium, after which it is removed or turned over. Subsequently, Sfi1-2 replaces or supplements this scaffold during an intermediate stage, followed by Sfi1-3 contributing to late-stage organization of the newly formed oral apparatus. We hypothesize that this stepwise scaffold handoff allows for stage specific remodeling of the cytoskeleton, enabling dynamic transitions in structural organization without compromising overall spatial integrity.

This mechanism is reminiscent of T4 bacteriophage assembly, where a temporary internal scaffold is used to shape the prohead (capsid precursor). The protein constituents of the assembly core, p22 and internal proteins, are gene products which are components of the phage head precursor but are not structural components of the finished capsid [64]. During bacteriophage morphogenesis, specific scaffold proteins are recruited in a temporal order, and once their role is fulfilled, they are proteolytically degraded or removed, allowing the structure to advance to the next stage. These scaffolds are essential for proper assembly but are not incorporated into the final mature virion. Similarly, in *Stentor*, different Sfi1 proteins may act as transient guides, sequentially shaping the growing primordium, but not necessarily remaining part of the final, completed oral apparatus.

In another case, ribosome biogenesis involves the stepwise assembly of ribosomal RNA (rRNA) and ribosomal proteins into mature ribosomal subunits. After transcription of rRNA and pre-rRNA processing and maturation, over 80 ribosomal proteins bind to pre-rRNA in a specific order, followed by subunit separation, export to the cytoplasm and final maturation [65]. Each step requires the previous step in order to proceed, much like how Sfi1-2 scaffolding is required before Sfi1-3 can scaffold the primordium.

Role of lateral filaments as potential circumferential positional cue

Classical studies on insect limb development have shown that when regions containing different positional cues are placed in proximity, it can trigger the formation of new organizing centers [66], development of ectopic structures, or in some cases intercalation of limb regions in inverted orientations [67]. Such observations point to mechanism for comparing positional information in neighboring regions so as to ensure continuity of form. Intracellular juxtaposition can likewise play a pivotal role in establishing defined positions in cellular patterning with *Stentor* providing a classic example. In *Stentor*, grafting pieces of the cortex with different stripe widths not containing an oral primordium site is sufficient to induce the formation of a new primordium [7]. This observation emphasizes the critical role of the juxtaposition of cortical regions with differing stripe widths appearing as a key organizing factor, with circumferential cues helping to establish a radial pattern that governs the location of oral primordium formation. However, the molecular basis for such circumferential positional information in *Stentor* are completely unknown.

Whatever the circumferential position information is based on, it correlates with stripe width which reflects the spacing between adjacent microtubule bundles (km fibers). Because the centrin cables are aligned with the microtubule bundles, stripe width thus also correlates with the spacing between longitudinal centrin cables. The spacing of the cables decreases as one moves counterclockwise around the cell when viewed from its anterior pole, terminating at the intersection of narrow and wide-spaced cables. This "locus of stripe contrast" defines the oral primordium site. When stripe contrast regions are created by surgical manipulation in different regions of the cell, they are sufficient to produce a new oral primordium, strongly suggesting that all cortical stripes contain some form of positional information.

Given that Sfi1 bands span the width between adjacent ciliary rows and show distinct expression patterns along the anterior-posterior axis, we propose that the length of these filaments may encode positional information. This model raises two questions. First, how are differences in the length of the Sfi1 bands read out to determine the site of primordium development, and second, how is a smoothly varying gradient of band lengths created. We currently have no answer to the first question, but we can propose a hypothesis for the second. It is known that the number of stripes increases with the size of the cell. Stripe multiplication can occur by splitting or "branching" where the widest pigment stripes begin to split when a new clear stripe of ciliary rows and fibrous structures emerges within the pigmented stripe. This growth process follows a spiral trajectory, with new short stripes added anteriorly and older stripes extending posteriorly, eventually reaching the posterior pole [2]. This would indicate that the newest ciliary rows are more tightly packed and shorter in length along the longitudinal

axis of the cell, compared to older stripes which are longer and more widely spaced. Sfi1 bands might thus reflect the developmental age of the ciliary stripes or serve as landmarks that may help establish circumferential identity across the cortex. If existing Sfi1 bands undergo gradual elongation over successive rounds of cell division, for example by incorporation of more Sfi1-centrin superhelical filaments, this would produce the observed circumferential gradient in filament length.

The potential role of Sfi1 bands as structural and spatial reference points is consistent with a model in which *Stentor* uses a cytoskeletal scaffold not just for mechanical support but for spatial patterning in which it integrates both longitudinal and circumferential positional cues to coordinate morphogenesis.

Conclusion

Our Sfi1 knockdown experiments demonstrate that loss of Sfi1 impairs not only oral apparatus regeneration but also whole-cell contractility, providing direct functional evidence that Sfi1 is required for both morphogenetic and mechanical processes. These findings suggest that in *Stentor*, Sfi1 links the molecular architecture of the cortex to the mechanical behavior of the entire cell, a role that likely evolved to support the unique demands of such a large, single-celled organism. Together, our findings suggest that spatial patterns at the sub-cellular level can be generated by spatiotemporal variation of scaffolding proteins that, in turn, organize structural proteins into distinct structures at the appropriate time and place during cellular development.

2.5 Materials and Methods

Stentor culturing and media

Stentor coeruleus cells were obtained from Carolina Biological Supply and grown in the dark, at room temperature in the lab. Cells are cultured in pasteurized spring water (Carolina Biological Supply). Cells are fed every 4-5 days with *Chlamydomonas reinhardtii* grown on TAP agar plates and resuspended in 15mL pasteurized spring water, with each 2qt culture being fed 5mL.

Molecular Phylogenetics

For the phylogenetic characterization of *Stentor* candidate centrin sequences, we gathered amino acid sequences of human and *Paramecium* centrin homologs using online BLASTP[68] and human centrin 2 as a query. We aligned them with *Stentor* sequences using MUSCLE (v3.8.425) and corrected the alignment manually by deleting gap positions and sequenced that could not be aligned properly. We used IQ-TREE2 (v2.2.0.3) with the Le-Gascuel substitution matrix and gamma distribution of among site rate-variation[69] and tested for robustness of the topology by running 1000 ultrafast bootstraps[70].

Sfi1 Analysis

Sfi1 homologs were identified in *Stentor* using BLAST[68], RADAR (Rapid Automatic Detection and Alignment of Repeats)[51] and ScanProsite[52]. Sequence logos generated from SteCoe_25973, SteCoe_10021, and SteCoe_17904 using WebLogo (Berkeley) showed the same sequence. Phylogenetic trees were generated using the Maximum Likelihood Method[71].

Antibody production

Pre-immune bleeds from rabbits were screened to avoid using rabbits previously infected with ciliated parasites that may produce antibodies that react with *Stentor* proteins. Screening was done by incubating western blots of *Stentor* proteins with pre-immune rabbit serum at a 1:500 dilution, then staining with secondary antibodies. Custom anti-Sfi1-1, anti-Sfi1-2, and anti-Sfi1-3 antibodies were generated and purified (Fortis Labs, Richardson TX) using the peptides RKKEDKNQVRKTP, MEGSKIPTLLED, ENIIRRTMRDADQR respectively. Antibodies were validated using a peptide block and immunofluorescence. Peptides were incubated at a 1:10 Ab:peptide ratio and incubated for 2 hours at room temperature.

Western blots

Lysate samples were prepared using 4X NuPage LDS sample buffer and run on Invitrogen Bolt bis-Tris Mini Protein Gels run in a Mini Gel Tank (Fisher Scientific

A25977) and transferred using the accompanying blotting module. HiMark™ pre-stained protein standard was used for Sfi1 western blots with high molecular weight, while PageRuler Plus Prestained protein ladder used in centrin western blots. Membranes were blocked for 1hr at RT with 3% BSA in PBST. Primary antibodies were diluted at 1:200 and incubated at 4C overnight. Secondary HRP antibodies were diluted at 1:1000 and incubated for 1hr at RT. Super Signal West Pico Chemi Substrate used for protein detection.

RNAi constructs

Sfi1 genes were amplified using PCR from *Stentor* genomic DNA isolated using a DNeasy Blood and Tissue Kit: Animal Blood Spin-Column Protocol (Qiagen, Germantown, MD). Ligation independent cloning was used to insert gene fragments into a pPR-T4p plasmid between two T7 promoters, and the vectors were transformed into Dh5a *E. coli* cells. Primer sequences and targeted regions are indicated in **Supplementary Table 2.2**. For negative controls, either empty pPR-T4p vectors containing no insertion or constructs cloned with the LF4 gene, which is involved in cilia length control but otherwise does not affect function or morphogenesis, were used.

RNA interference

RNAi was either performed by feeding[72] or microinjection. Feeding constructs were transformed into HT115 *E. coli* and grown to OD 0.4-0.6, then induced with 1mM

isopropyl-β-d-thiogalactopyranoside (IPTG) and incubated shaking overnight at room temperature. *Stentor* were fed daily with resuspended bacteria pellets for 7 days. Wells were cleaned and replaced with fresh Carolina Spring Water every other day. Microinjection protocol was adapted from Slabodnick, 2023 (unpublished). Briefly, 70-100 cells were placed in chambered slides containing 2mL 1.5% methylcellulose. Cells were allowed to acclimate and fully extend. Drummond Borosilicate glass capillaries (3-000-203-G/X) were siliconized using Sigma Aldrich SigmaCote (SL2) and allowed to air dry. Capillaries were pulled using a Sutter micropipette puller (P-97) and needles were cut with a razor blade. RNA was loaded into needles using Microloader pipette tips (Calibre Scientific). RNA was synthesized using NEB HiScribe T7 High Yield RNA Synthesis kit (E2040S) using linearized pPR-T4p vector with cloned constructs as the template. RNA was concentrated and cleaned using NEB Monarch Spin RNA Cleanup Kit 500ug (T2050L) and microinjected at 800-2000ng/uL using a Drummond Nanoject II microinjector.

Regeneration Assay

Sucrose shock regeneration assay is adapted from Lin (2022). Briefly, *Stentor* were concentrated in 1mL in a 50mL conical tube. 1mL 30% sucrose (Sigma Aldrich S7903) was added for a final concentration of 15% and gently mixed. Cells were inspected visually for 1:10-2:00 minutes until the membranellar bands had fallen off. Cells were washed three times in pasteurized spring water (Carolina Biological Supply) to remove sucroce and visually staged at 4-, 6-, 8-, and 24-hours post sucrose shock. For easier

staging, 20-30 cells were placed in a 9mm spacer (Grace BioLabs) on a microscope slide, sealed with a 18x18 glass coverslip and observed under a Zeiss AxioZoom V16 microscope.

For regeneration after bisection, cells were cut in half as previously described[73]. Cells were placed in 0.25% methylcellulose on parafilm and cut with a glass needle. Posterior and anterior halves were separated and washed three times to remove methylcellulose.

Immunofluorescence and Expansion

Cells were fixed in freezing methanol (Sigma Aldrich 67-56-1) overnight and rehydrated in methanol in 0.5x PBS for 20 minutes. Cells were washed 3 times with 0.1% TBS-Triton X and blocked in antibody dilution buffer containing 2.5% BSA (Sigma Aldrich A030), 0.5% cold water fish gelatin (Sigma Aldrich G041), 0.1% Triton X in PBS overnight at RT. Primary antibodies were added using the following dilutions: Centrin 20H5 (Sigma Aldrich 04-1624) 1:100, Sfi1-1-3 1:100, and Actub 6-11B-1 (Sigma Aldrich T7451) 1:1000 and incubated for 1 hour at RT and washed 3x with TBS-Tx. Secondary antibodies goat anti-mouse 488 (Invitrogen A-11001), goat anti-mouse 594 (Invitrogen), goat anti-rabbit 488 (Invitrogen) and goat anti-rabbit 594 (Invitrogen) were used at a 1:200 dilution and incubated for 1 hour at RT. Cells were then washed 3x with TBS-Tx. Cells were mounted in Prolonged Glass Antifade (Invitrogen P36980) and placed inside a 9mm SecureSeal spacer (Grace BioLabs) adhered to a microscope slide and sealed with a 18x18mm glass coverslip. For expansion samples, cells were fixed and stained as described above. A modified Magnify[54] expansion protocol was used for expansion.

Briefly, fixed cells were mounted on poly-lysine coated 8mm round coverslips (Thomas Scientific 127H20) and embedded in the Magnify gel monomer solution overnight at 37C in a humidified chamber. Gels were carefully removed and placed in an Eppendorf tube with 1mL Magnify homogenization buffer and incubated at 80C for 24 hours. Gels were washed in 1xPBS. Gels were stained again using 2x the antibody concentration used in pre-gelation samples diluted in 2% BSA in PBS at RT for >2 hours. After washing 3x 10min each in 1xPBS, DyLight 594 NHS Ester (Thermo Scientific PI46413) was added at 20ug/mL in addition to any other secondary antibodies used. Gels were washed 3x10min in 1xPBS and expanded twice for 30min each in ddH20, then expanded once more overnight. Gels were imaged in Ibidi 2-well slides and imaged using confocal microscopy.

Imaging

Brightfield imaging was done using Zeiss AxioZoom V16 equipped with a Nikon Rebel T3i SLR Camera. Confocal microscopy was done using CSU-W1 Spinning disk equipped with an Andor Zyla sCMOS camera. High speed imaging was done using Vision Research v7.3 or v341 high speed cameras.

Contraction Assays

Pipetting Assay: Fully extended free-floating or anchored cells were pipetted into a P20 pipette tip, which induced contraction in control cells. Each cell was not assayed more than once to prevent habituation.

High-Speed Contraction Assay: Individual cells were imaged in a 9x9 SecureSeal spacer (Grace BioLabs) adhered onto a microscope slide and sealed with a glass coverslip. A mechanical force onto the side of the slide was used to induce contraction of fully extended cells.

Electrical Pulse Assay: *Stentor* cells were stimulated to contract using an electrical pulse. A 555 timer-based one-shot pulse generator (a kind gift from Joseph Lannan) with a potentiometer (Bourns Inc 2590S-2-103L) was attached to glass slides with flat pieces of metal obtained by breaking a double-edged razor blade into fourths, on the longitudinal sides functioning as both electrodes and spacers. These pieces of metal and vacuum grease created a chamber in which 20-50 cells in 1.5% methylcellulose were placed and gently compressed with a coverslip. The methylcellulose along with the compression from the coverslip helps to promote full extension of the cells. Images before and immediately after the electrical pulse were taken using a USB microscope (Celestron Handheld Digital Microscope Pro).

2.6 Supplementary Figures

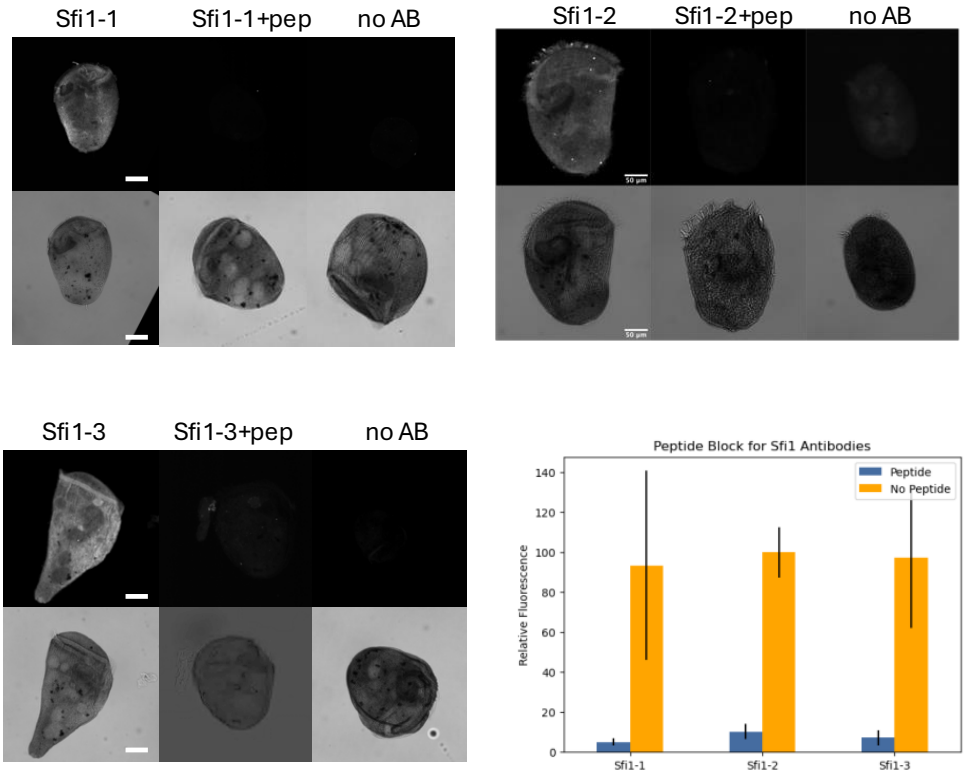

Figure 2.8: Peptide block of Sfi1-1, Sfi-2, and Sfi1-3 antibodies. Antibodies were pre-incubated with their corresponding peptides. Immunofluorescence shows little or no fluorescence with peptide blocked antibodies (n=13) compared to controls (n=12). Scale bar 50um.

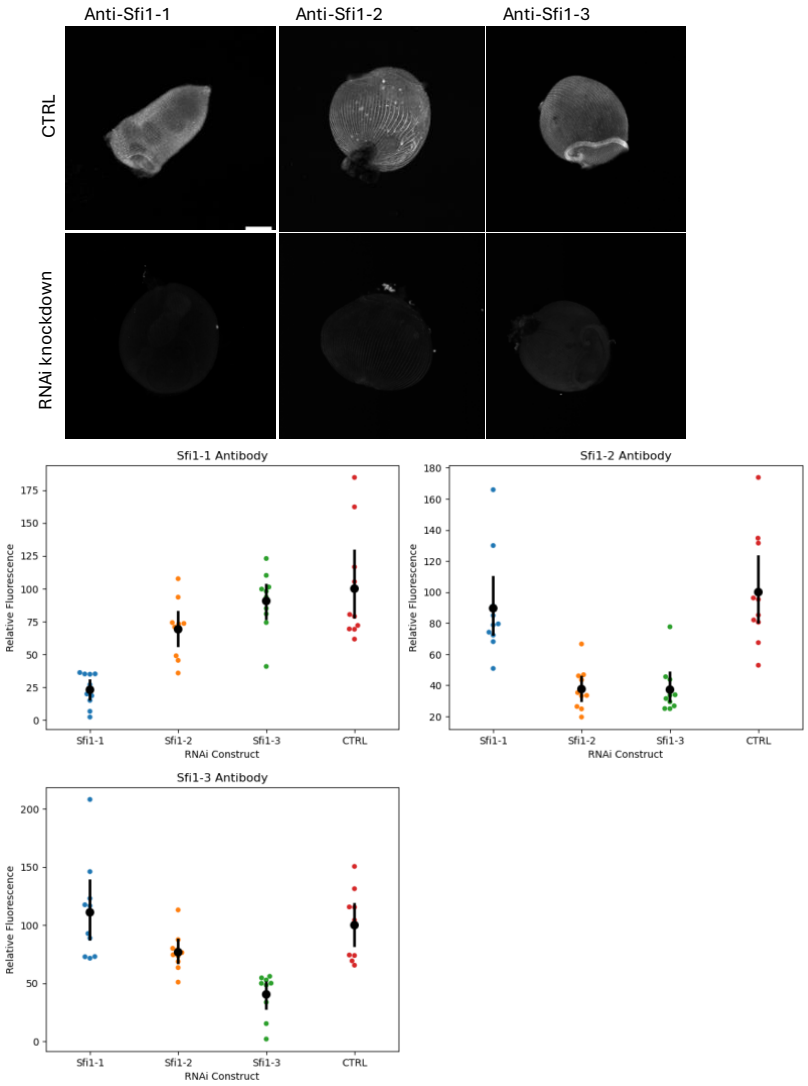

Figure 2.9: RNAi knockdown validation of each Sfi1 antibody.

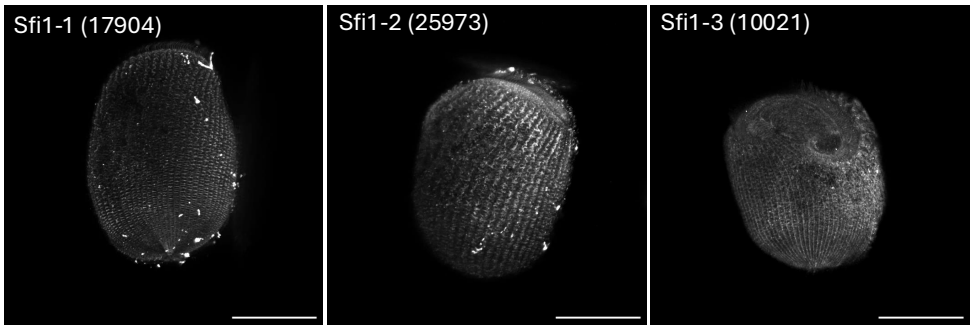

Figure 2.10: Representative fluorescence images of each Sfi1 antibody

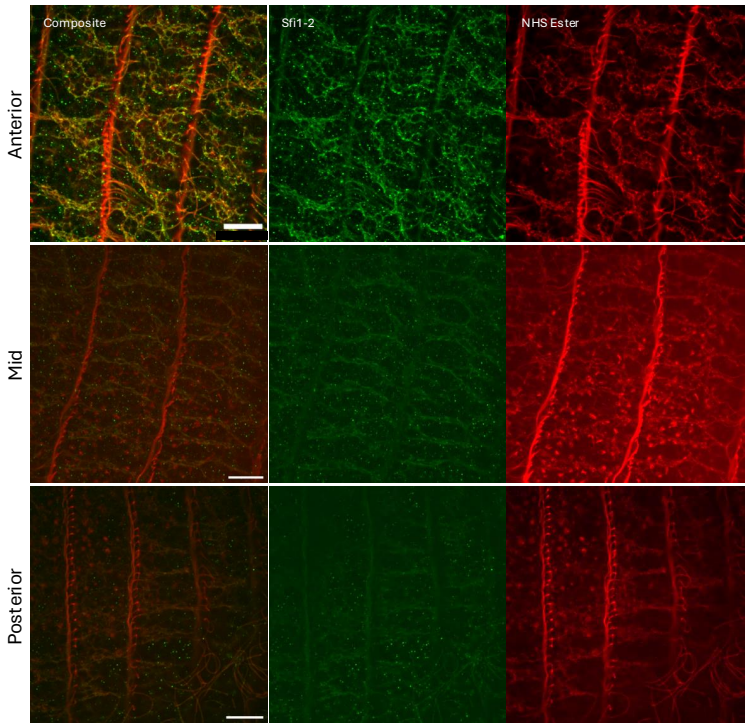

Figure 2.11: NHS-Ester stains Sfi1 structures. NHS-Ester stains Sfi1 structures more clearly in the posterior of the cell compared to Sfi1-2 antibody (green).

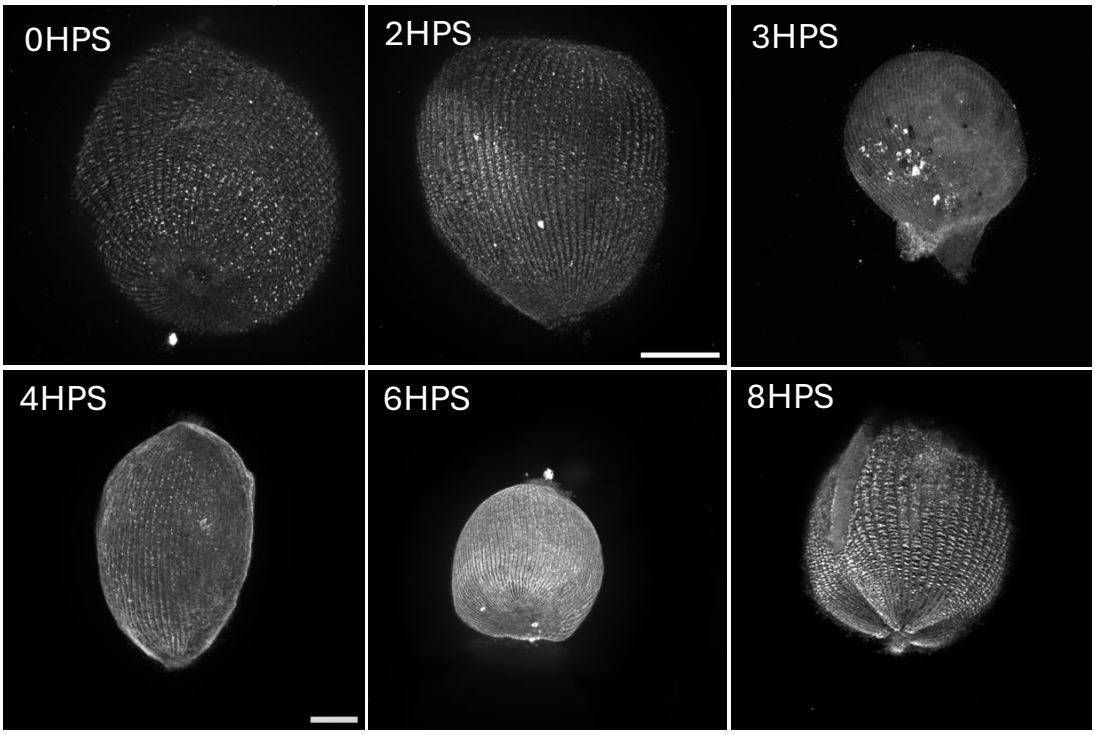

Figure 2.12: Re-establishment of Sfi1 lateral bands during regeneration. Bands appear more punctate until fluorescence is only in the cortical rows at 3HPS. Bands begin to reappear and re-establish by the end of regeneration.

Supplementary Table 2.2 List of RNAi construct primers

Construct	Length (bp)	Region of RNAi target	Forward	Reverse Primer
Sfi1-1	1382	2904-4285	TCGTGACGCATTTCAAAGAG	TCTTGCATTTGCAGTCTTGG
Sfi1-2	1372	1226-2597	CCCACCACAGAGTTGATGTG	CTTCTGGCTGTTGCTTTTCC
Sfi1-3	1462	7250-8711	ATGGCAAAGATCAAGCATCC	GTCAATGATGTCCGTATGCG
Mob1	633	40-672	AAGAAGCGAATTGAAAAAGGCCAGC	GTTACCAGAAGCTTCTCTTTCCATTCTTTCC
LF4	876	8-884	CAGAATACCGTTTGATATCAAAAAAAGGTGAAGG	CTACTTGCCTCATCAACAAAATCTTTGAAATAAGG

CHAPTER 3: CELL CYCLE MACHINERY IN *STENTOR* REGENERATION

3.1 Abstract

Regeneration in *Stentor coeruleus* not only involves the reassembly of complex structures such as the oral apparatus but also recapitulates many of the morphogenetic events typically associated with cell division. This overlap suggests that *Stentor* may repurpose components of the cell cycle machinery to regulate regeneration, raising the central question: is regeneration a distinct process, or is it a re-activation of developmental pathways?

Unlike most eukaryotic cells that pass through clearly defined phases ($G_0 \rightarrow G_1 \rightarrow S \rightarrow G_2 \rightarrow M$), *Stentor* cells exhibit an atypical cell cycle. They are binucleate and polyploid and are predominantly in interphase, characterized by continuous DNA synthesis, and divide amitotically every 1-2 days [2]. Synchronization of their cell cycles is difficult, which complicates conventional analysis of timing-related processes. Despite this, evidence increasingly points to shared regulatory components between the cell cycle and regeneration programs. Previously, it has been suggested that *Stentor* cells are either in a state of activation or inhibition, which may correlate to cell cycle stages.

A key signaling pathway of the cell cycle involves the Rb-E2F-DP1 module, a well-conserved pathway that governs G_1/S transition in many eukaryotic systems.

Canonically, CDK4 phosphorylates Rb, releasing the transcription factor E2F to activate genes required for DNA synthesis and cell cycle progression.

Transcriptional analyses of regenerating *Stentor* cells have identified the E2F homolog, SteCoe_12750, which is upregulated early in the regeneration process. Intriguingly, this gene remains expressed even in the presence of cycloheximide, which blocks translation, suggesting that it may be a primary response gene in the regenerative signaling cascade [8]. This gives up a starting point in determining how regeneration is initiated, as we can look at molecular players upstream of E2F.

Pharmacological inhibition of CDK4 using Palbociclib has provided compelling evidence for the role of cell cycle regulators in regeneration. When CDK4 activity is blocked, downstream targets of E2F fail to be transcribed, and cells exhibit impaired regenerative progression, particularly in the later stages of oral primordium maturation. In Palbociclib-treated cells, bulk RNA-sequencing revealed downregulation of canonical cell cycle regulators, including Rb, cyclins, and CDKs, while phosphoproteomic profiling of cells 1HPS and treated with Palbociclib hint at what may be upstream of CDK4. These findings imply that E2F functions as more than just a cell cycle regulator; it may act as a molecular switch that links external injury or developmental cues with a coordinated transcriptional response that initiates regeneration.

Thus, *Stentor* provides a powerful model for exploring how core cell cycle machinery can be repurposed for non-canonical functions like regeneration. This suggests a broader principle in the biology of regeneration, that regeneration relies on the strategic

redeployment of developmental programs, regulated in a spatiotemporally controlled manner in addition to unique factors.

3.2 Introduction

A key question in the biology of regeneration is what triggers the process? In some multicellular species, such as Hydra, studies indicate that apoptosis acts as a signal to stimulate proliferation within the regenerative tissues, producing the cells needed for full regeneration[74]. In invertebrates with remarkable regenerative capacity, like planarians, regeneration is largely fueled by the differentiation of plentiful adult pluripotent stem cells [75]. In contrast, many other organisms rely on the reactivation of gene-regulatory networks that were active during embryonic development, even within terminally differentiated cells. However, regeneration also differs from development in many ways, including the use of regeneration-specific cell types and gene regulatory networks.

But how do individual cells initiate regeneration? It has been suggested that *Stentor* cells are either in a state of activation or inhibition, and these states counteract each other. A general rule from classical regeneration and embryological studies is that formed parts inhibit new formations of the same type [76], [77]. Indeed, this has been shown in *Stentor* through grafting experiments. However, in experiments where the oral apparatus remained intact, but was rotated 180 degrees, a primordium still formed, showing that discontinuities in the microtubule fiber tracks of the *Stentor* cortex can

initiate the assembly of basal bodies to the primordium site and subsequent oral development [56]. This shows that it may be the proper pattern and relationship to the whole cell that is essential for the inhibitory effect, and that the inhibitory substance is not diffusible [56]. Through grafting experiments, Tartar determined that these inhibitory and activating states are able to spread between cells, and that if regenerating cells are grafting to non-differentiating cells either, the non-differentiating cell will either begin to form a primordium, or the regenerating cell will absorb its primordium, depending on the stage of the primordium on the regenerating cell. The further developed the primordium, the state of activation becomes lower, and inhibition increases. Evidence for differential growth in the cortical fibers has also been shown to trigger oral development, however, the molecular mechanisms behind this process are unknown. One method of investigating this is to look at what is upregulated early in regeneration and move upstream to find the trigger of regeneration.

Previously, transcriptional programs of regeneration in *Stentor* show that transcriptionally, up to the first 30 minutes post removal of the oral apparatus is similar to that of a non-regenerating cell [8], [11]. Among the early expressed genes, the transcription factor E2F was identified as an early regulator of regeneration in *Stentor coeruleus*, particularly during the regeneration of anterior structures such as the oral apparatus [8]. Temporal analysis shows that E2F is expressed in cells responding to sucrose shock and in posterior half-cells regenerating anterior parts, but not in anterior halves regenerating posterior tails. Notably, E2F is upregulated even in the presence of cycloheximide, indicating that it may act as an early-response gene initiating subsequent waves of gene expression [8]. Promoter motif analysis identified 13 putative E2F target

genes, whose expression is tightly clustered within a one-hour window coinciding with the expression of centriole-related genes and the E2F ortholog, E2F-1. Of these, 12 targets showed reduced expression upon cycloheximide treatment, supporting their dependence on new transcription likely driven by E2F, while one gene, *SteCoe_2152*, maintained normal expression. The majority of these targets fall into expression cluster 2, with none in cluster 1, which includes genes repressed during regeneration, suggesting that E2F primarily functions as a transcriptional activator in this context. Although the predicted targets span multiple functional categories, they include cell cycle–related genes such as cyclin and a cyclin-associated protein, consistent with E2F's known role in cell cycle regulation. Importantly, these E2F targets are upregulated only during anterior regeneration, further indicating a specialized role for E2F in directing regeneration of complex anterior structures rather than general wound healing.

The E2F transcriptional factors are key regulators of cell cycle progression in many eukaryotes. E2F complexes are defined by their ability to bind to a sequence element that was identified originally in the adenovirus E2 promoter [78], [79], [80]. There are multiple groups of E2Fs, mainly activators, inhibitors, and repressors. Canonically, as cells enter the cell cycle and approach the G1/S transition, activating E2F and its heterodimerization partner DP1 are bound by retinoblastoma protein (Rb), inhibiting transcription of E2F targets. Rb dissociates from activating E2Fs upon being phosphorylated by the cyclin-dependent kinase (CDK) complexes, allowing target gene activation and thus progression in the cell cycle.

In *Stentor*, the process of cell division and oral regeneration look strikingly similar, in that they undergo the same morphological processes **(Figure 1.2)**. In both cases, basal

bodies assemble at the primordium site, forming a primordium which elongates and curves at the posterior to form the gullet, then migrates to the anterior position of the oral apparatus. Additionally, morphological changes in both cases are seen in the macronucleus, which condenses and remodulates at the end of the process. This suggests that there is some link between regeneration and cell division, since they look morphologically similar, and cell cycle genes appear to be involved in both these processes.

Here, we describe a possible model for how regeneration and cell division may be triggered and show that the E2F pathway is required for regeneration, as well as proliferation, likely acting as an activator. We also show that CDK4/6 temporally controls regeneration, and DNA synthesis during regeneration follows a pattern similar to that of DNA synthesis during cell division.

3.3 Results

Sender receiver model for initiation of the oral primordium

Based on previous grafting and microsurgical experiments investigating how oral primordium growth is initiated, we have proposed a sender-receiver model for how this occurs in *Stentor* cell division and oral regeneration. Sender-receiver models are common in biology, such as in morphogen gradients in *Drosophila,* where localized transcription of *bicoid* mRNA in the anterior of the embryo needs to diffuse through the cytoplasm to nuclei along the anterior-posterior axis [81]. The gradient needs to remain

intact to properly repress or activate downstream targets, otherwise patterning breaks down. In *Stentor*, because we know that the inhibitory substance likely resides in the cortex, and that discontinuities in the cytoskeleton can trigger oral primordium formation, we propose that *Stentor* use microtubule tracks of the cortex to transport an inhibitory signal from the "sender", the oral apparatus, to the "receiver", the oral primordium site. If these tracks are disrupted, the signal can no longer be sent, thus allowing a state of activation to take over the state of inhibition. In regeneration, because the oral apparatus is removed, this eliminates the sender and allow for oral primordium formation. In cell division, when *Stentor* cells grow, the volume of the cell increases, but not the size of the oral apparatus. Thus, it could be reasoned that the increase of cytoplasmic volume compared to a proportionally smaller oral apparatus has decreased the inhibitory signal enough such that activation takes over. Additionally, we know that cortical breakage can occur during growth, possibly disrupting the microtubule tracks required for transporting the inhibitory signal. However, we do not know what the molecular identities of the signals in each of these roles. Given the expanded *Stentor* kinome [82], one possibility is that the sender is a kinase that phosphorylates the signal, which is then transported via motor protein to the primordium site.

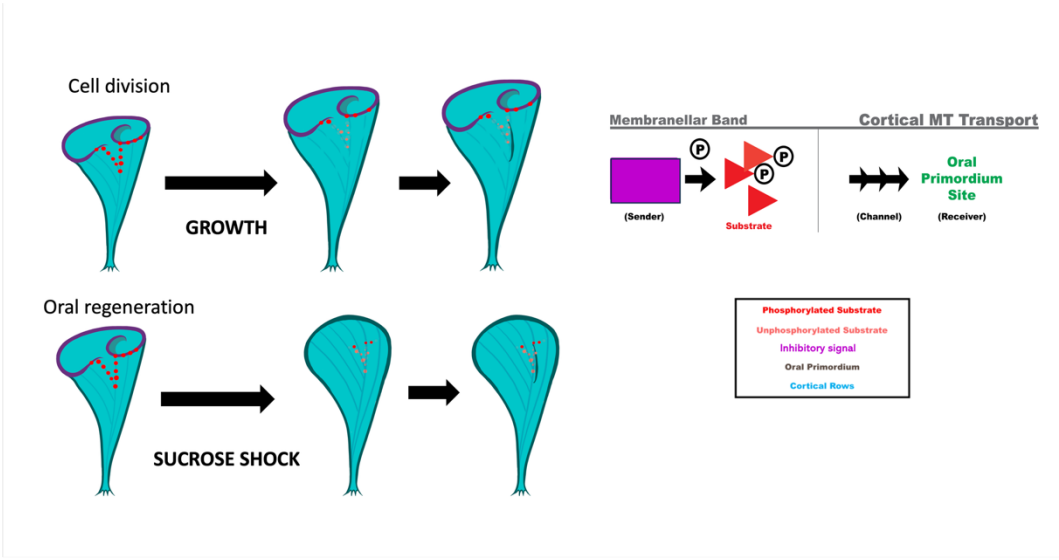

Figure 3.1: A sender-receiver model for oral primordium formation. An inhibitory substance resides in the membranellar band which phosphorylates a substrate, which travels through the microtubule cortex to the oral primordium site. In cell division, growth causes disruptions in the MT track and in regeneration, the membranellar band along with the sender is removed.

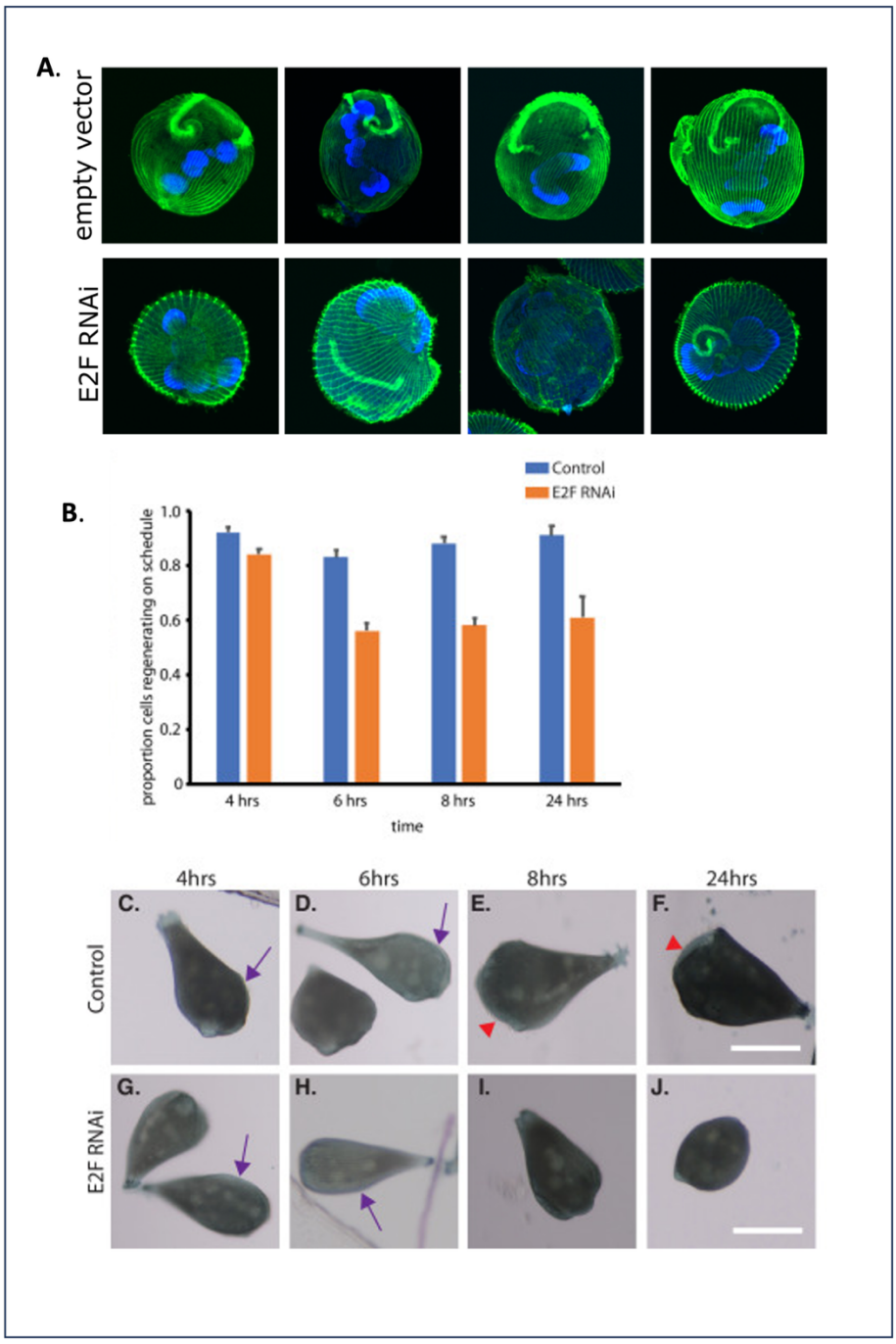

Figure 3.2: E2F is required for regeneration (A) Representative images acetylated tubulin immunofluorescence of E2F RNAi cells 8HPS and empty control cells 8HPS. E2F RNAi cells do not form a complete primordium with a gullet, but either have no primordium, partial primordium, or small band with no gullet. (Figure caption continued on next page.)

(Figure caption continued from previous page.) (B) Quantification of E2F RNAi and control cells at the correct stage during a timecourse of regeneration. (C-F) Representative images of control cells during regeneration. Purple arrow indicates primordium; red arrowheads indicate complete oral apparatus. (G-J) Representative images of E2F RNAi cells during regeneration. No visible oral apparatus is seen at 8HPS.

E2F is required for regeneration and proliferation

We tested whether E2F was functionally important for oral regeneration using RNAi directed against the upregulated E2F ortholog SteCoe_12750. In E2F RNAi-treated cells, the oral primordium formed normally after sucrose shock, but failed to progress or be maintained, such that by 8HPS, many of the cells were missing either an oral primordium or fully developed OA. Even after 24HPS, many RNAi cells lacked any sign of OA or primordium. Taken together, our results indicate that oral regeneration proceeds normally for the first 4HPS but then fails to proceed in later time points.

We next observed how often E2F RNAi cells divide compared to controls. E2F RNAi cells were tracked for 5 days after 5 days post-injection. This allowed time for the RNAi phenotype to develop and ensured the phenotype would last throughout the testing period. A single cell was placed in a well and number of cells in each well was counted after 5 days. 24 cells from each condition were analyzed and showed that the E2F RNAi cells did not proliferate as often as the LF4 control cells. At the end of the experiment, the average number of control (LF4) cells in each well was 8.5, while it was only 3.8 in E2F RNAi wells.

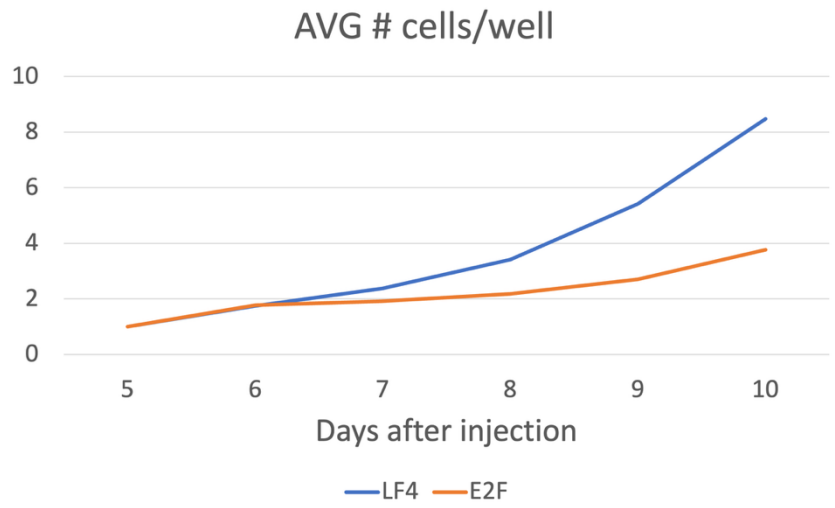

Figure 3.3: E2F RNAi have decreased proliferation. Average number of cells per well after 5 days post injection. After one day (Day 6) the rate of division in E2F RNAi cell is significantly decreased compared to LF4 controls.

One possible model for why E2F RNAi cells might be dividing less often is the Rb dilution model. Lower CDK4/6 activity results in less Rb being inactivated, thus the cell continues to grow instead of divide. We then tested this model by measuring the area of cells flattened between the microscope slide and the coverslip. We found that these measurements between the control (n=137) and E2F RNAi cells (n=78) was not significantly different, thus the cell does not noticeably grow in size from knockdown of E2F. This could be because E2F is downstream of Rb and CDK4 and should be repeated using Palbociclib, which inhibits CDK4/6.

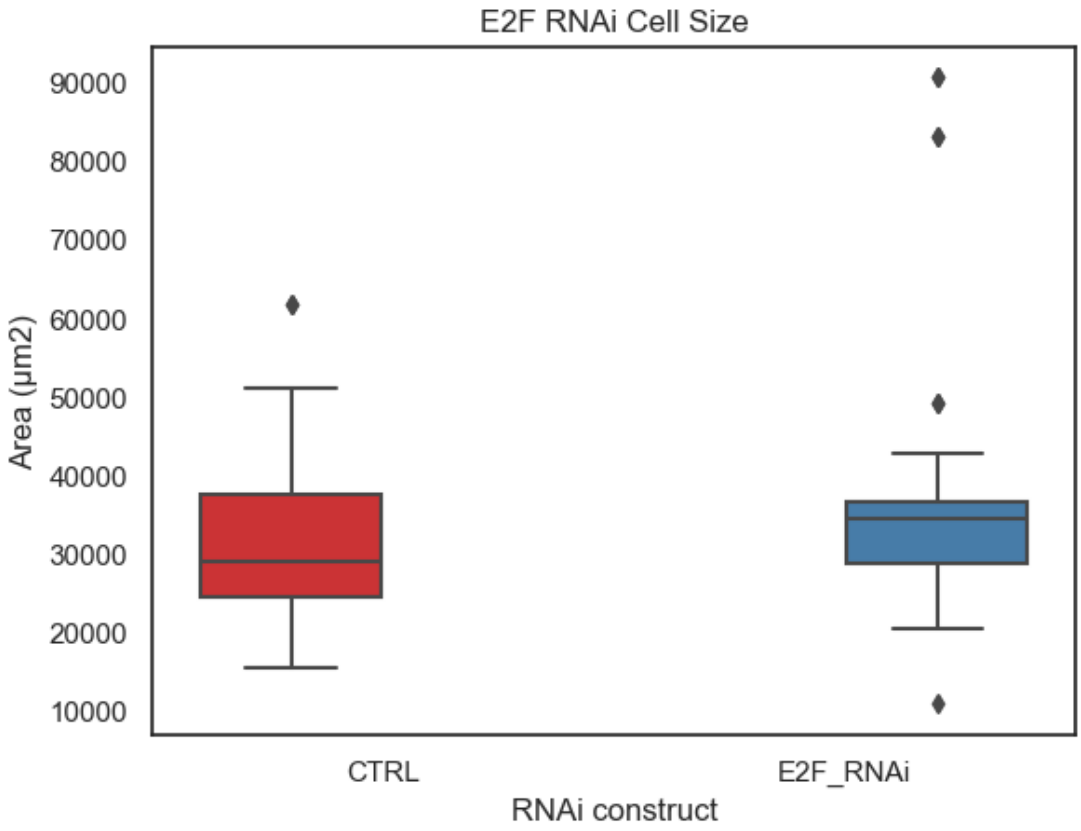

Figure 3.4: Area of flattened cells. There is no significant difference between control (31293±9305um²) and E2F RNAi (35582±13498um²). Significance measured by t-test, p>0.05.

Temporal control of regeneration by CDK4/6

We next tested to see if CDK4/6 inhibition produced the same phenotype as E2F RNAi by using the inhibitor Palbociclib during regeneration **(Figure 3.6)**. We staged the cells at 8HPS, where cells should be at Stage 2 by 4HPS, Stage 3 at 6HPS, and Stage 4 at 8HPS. Stage 1 corresponds to a cell with no mouthparts, stage 2 has a visible primordium, stage 3 has a gullet, and stage 4 is fully regenerated. Indeed, cells largely did not have a primordium at all, it was reabsorbed by 8HPS, or it had some visible

primordium compared to RNAi and DMSO controls which mostly fully regenerated by 8HPS. The phenotype from Palbociclib was slightly stronger, likely due to incomplete knockdown by RNAi **(Figure 3.5, 3.6)**. At 8HPS, 50.6±24% (8 replicates, n=16-64) E2F RNAi cells fully regenerated, 28.7±19% (10 replicates, n=30-100) Palbociclib treated cells regenerated compared to 87.9±8.6% (8 replicates, n=49-115) RNAi controls and 91.9±4.2% (10 replicates, n=25-54) DMSO controls.

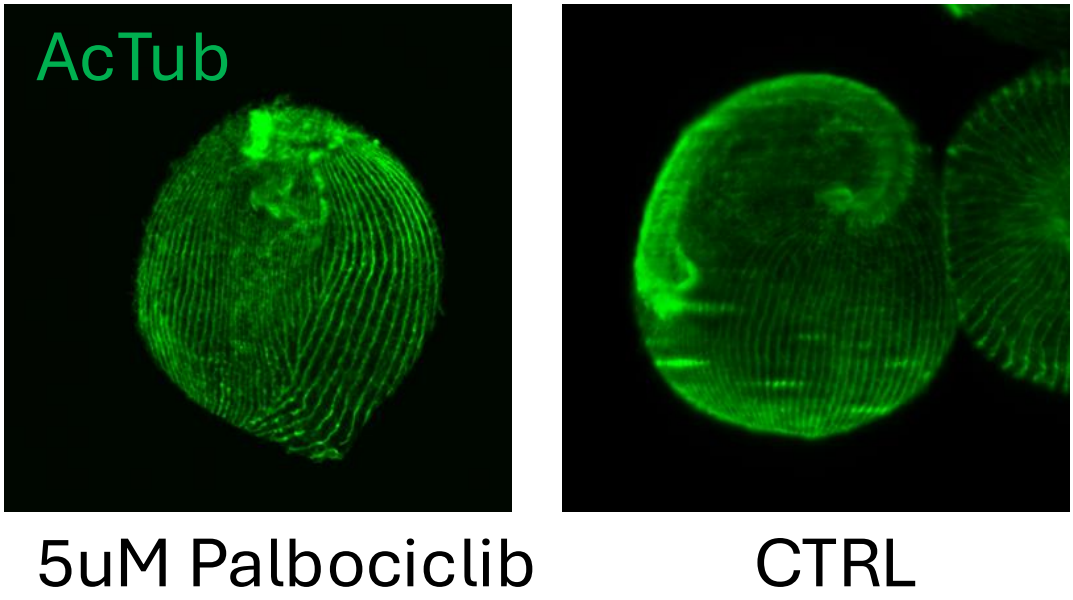

Figure 3.5: Palbociclib treated cells do not maintain an oral primordium. Representative images of immunofluorescence of Palbociclib treated and control cells 8 hours post sucrose shock.

Next, we tested to see if the Palbociclib treated cells could continue to regenerate if Palbociclib was washed out at 4HPS **(Figure 3.7A)**. In three independent experiments, we found that when we wash out Palbociclib at 4HPS, 81.5±1.6% of cells fully regenerated, compared to treated cells not washed out (n=34-50, 17.5±7.8%). Control

cells with a wash and no wash regenerated n=15-36, 98.8±2.1% and n=27-33, 100% respectively. While the proportion of cells after the washout that regenerated was much greater, it is still significantly different from the controls. However, this could be because of a delay after the drug is washed out, for the cell to resume primordium growth. Later timepoints will be necessary to determine if these cells continue regenerating past 8HPS. We also tested how Palbociclib affects cells temporally during regeneration. To do this, we added Palbociclib to regenerating cells at different timepoints **(Figure 3.7B)**. We added 5uM Palbociclib at 0HPS, 4HPS, and 6HPS. Very few cells regenerated when the drug was added at 0HPS (n=30 5.5±5.1%). When added slightly later at 4HPS (n=31-38, 20.5±7.4) that percentage increases, and again at 6HPS (n=30, 35.6±3.3%), compared to no inhibitor controls (n=30, 93.4±3.3%). This result shows that earlier timepoints are more sensitive to CDK4/6 inhibition by Palbociclib.

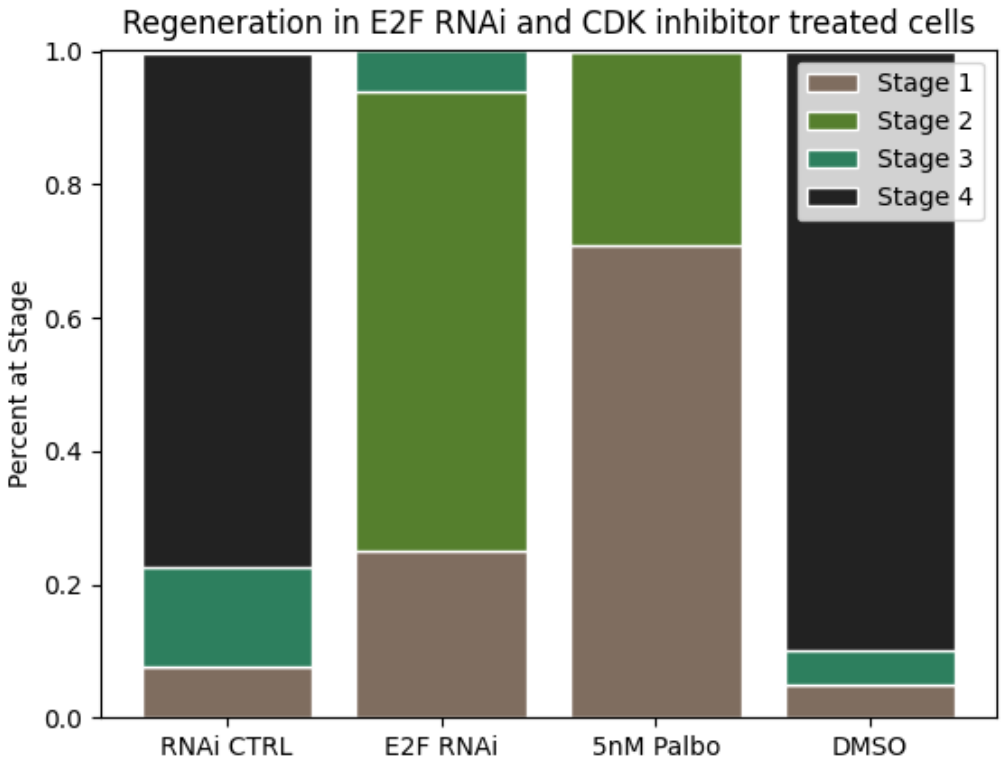

Figure 3.6: E2F RNAi and Palbociclib treated cells exhibit similar phenotypes. Cells largely remaining in stage 1 or stage 2, where stage 1 denotes a cell with no mouthparts, stage 2 a cell with a visible primordium, stage 3 with a visible gullet, and stage 4 fully regenerated.

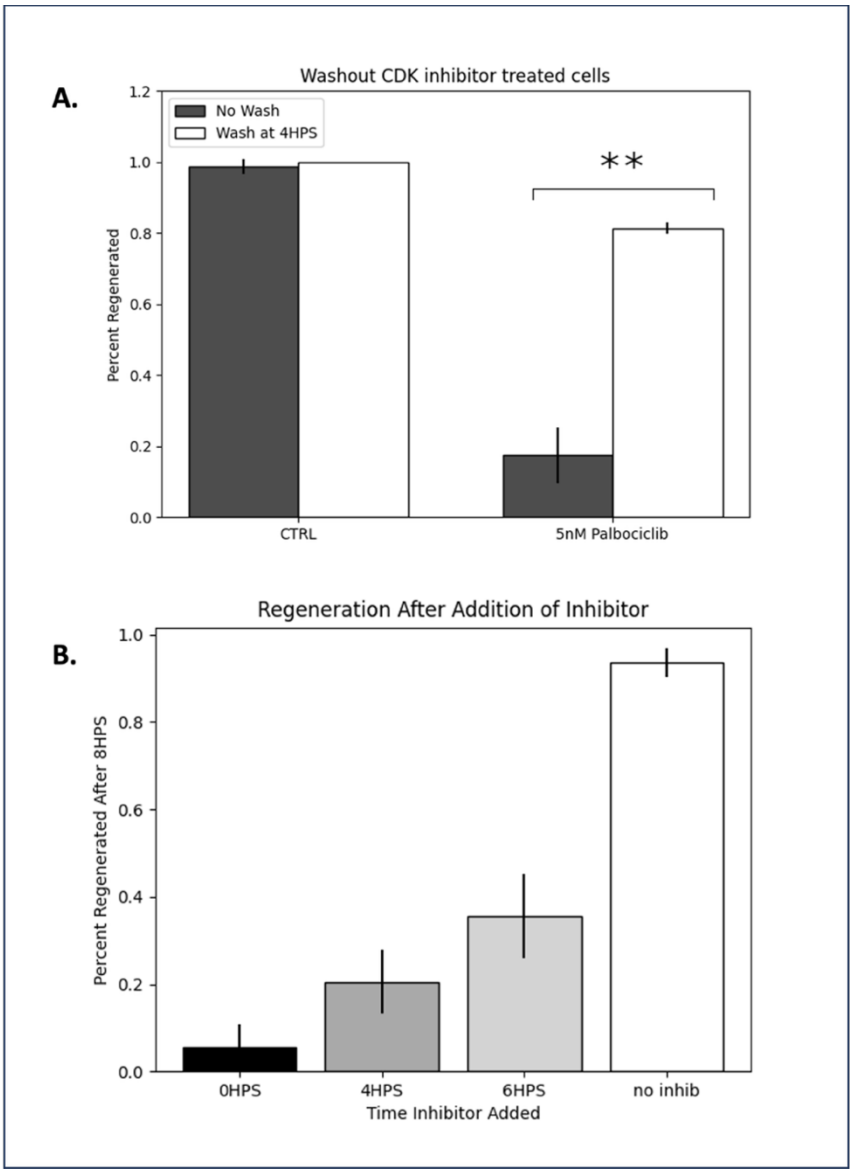

Figure 3.7: Temporal control of regeneration by CDK4/6 (A) Quantification of cells that regenerated after Palbociclib washout at 4HPS. (B) Quantification of cells that regenerated after Palbociclib was added at different timepoints. The earlier the inhibitor is added, the more severe the phenotype.

DNA synthesis during regeneration

What cell cycle phase correlates with the activated cell state? Using an Edu incorporation assay paired with click chemistry imaging, we looked at synthesizing DNA in regenerating cells. Cells were incubated with 100uM Edu for 30 minutes at every hour for 10 hours with n=36-110 cells per timepoint. Because *Stentor* cells are too large for flow cytometry, individual cells have to manually be analyzed, thus the low number of cells per timepoint, and more data is required to make any conclusions. We find that at the onset of regeneration DNA synthesis decreases until E2F is upregulated at 1.5HPS. DNA synthesis increases slightly until 4HPS and decreases when the macronucleus compacts at 5HPS and remains low until regeneration is completed **(Figure 3.8)**. The initial decrease in DNA synthesis is consistent with the idea that non-morphogenetic E2F knockdown cells (n=91) remain in S phase, we might expect to see more DNA synthesis occurring in these cells, however, we do not see a significant difference in Edu incorporation compared to control cells (n=131) **(Figure 3.9)**. However, because our cells cannot reliably be synchronized, a portion of our "non-morphogenic" cell population will be in the process of dividing, and thus not in S phase. Therefore, the level of DNA synthesis of the non-morphogenic cells appears to be increased from if the cells were synchronized and all in S phase, and we cannot necessarily conclude that E2F RNAi cells do not have an increase in synthesizing DNA, because they remain in S phase longer than control cells.

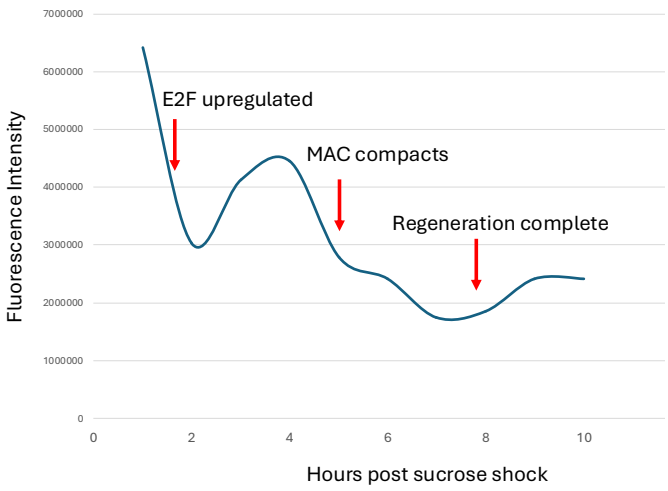

Time 0 = average of unsynchronized vegetative cells
HPR (hours post regen) = HPS+8

Figure 3.8: Time course of Edu incorporation during regeneration.

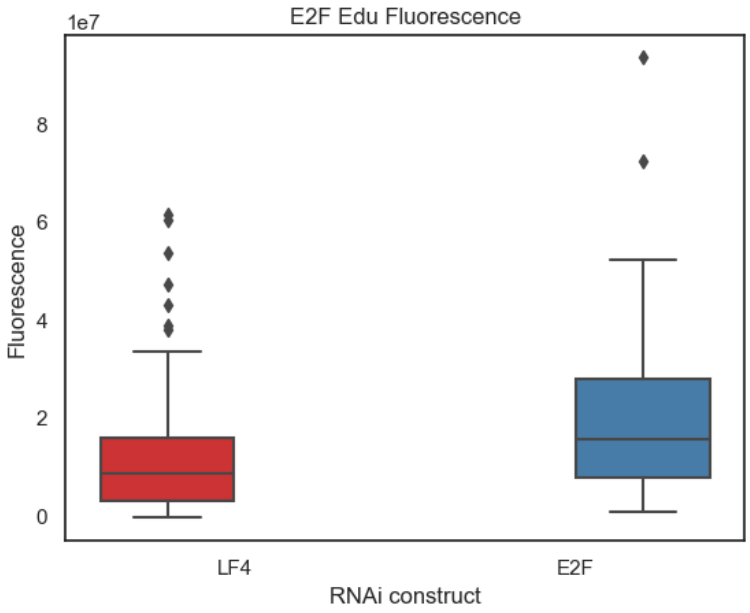

Figure 3.9: E2F knockdown cells do not significantly synthesize more DNA compared to control (LF4) cells.

RNA sequencing and phosphoproteomics

To investigate early molecular responses during regeneration, we performed bulk RNA sequencing on. Cells were treated with Palbociclib at 2HPS and compared to untreated control cells at the same time point. Palbociclib treatment allowed us to probe the role of G1/S cell cycle regulators by selectively inhibiting CDK4 activity during early stages of regeneration. Our analysis revealed a notable downregulation of key cell cycle regulators, including E2F, Rb, and multiple cyclins, all of which are essential components of the G1/S progression machinery **(Table 3.1)**. The transcription factor Myb, also known to function at the G1/S checkpoint, was reduced in expression as well **(Table 3.1)**. These results support the idea that cell cycle entry is linked to the initiation of regeneration, suggesting that Palbociclib effectively suppresses this regenerative entry program at the transcriptional level.

We also observed downregulation of E2F target genes **(Table 3.1)**, including a member of the alpha/beta hydrolase family, suggesting that E2F activity is functionally impaired in Palbociclib treated cells and that its downstream gene network is disrupted. These findings show that E2F acts as a key effector of regenerative transcriptional activation, downstream of CDK4/Cyclin D.

To complement these transcriptional findings and identify early signaling events upstream of transcriptional control, we performed phosphoproteomic analysis to assess dynamic phosphorylation changes occurring at 2HPS. Among potential phosphorylation changes was a mitogen-activated protein kinase (MAPK), a well-known regulation of cell proliferation, stress responses, and development in other systems [83]. Transcriptional

regulation of cell cycle components by MAPs links CDKs to the MAP kinase cascade, as MAPKs regulate the expression of D-type cyclins. The identification of MAPK phosphorylation at this early time point provides compelling evidence that it may act as an initial signaling cascade in triggering the regeneration gene expression program.

Table 3.1: E2F pathway genes downregulated in Palbociclib treated cells

Accession	Annotation
SteCoe_15560	Rb
SteCoe_7783	CDK4/CDK2
SteCoe_4387	Cyclin A2
SteCoe_31478	Cyclin
SteCoe_23651	Cyclin
SteCoe_23514	Cyclin B2
SteCoe_14065	Cyclin (G2/M specific)
SteCoe_12190	Cyclin
SteCoe_11470	Cyclin
SteCoe_9926	E2F
SteCoe_2128	E2F target – hypothetical
SteCoe_18056	E2F target – alpha/beta hydrolase
SteCoe_2151	E2F target - hypothetical

3.4 Discussion

Regeneration and cell cycle genes

It has been previously established that a number of genes expressed during regeneration and genes encoding cell cycle-related proteins [8], [11], [55]. One hypothesis to explain this expression is that cell cycle machinery might help regulate the timing of regeneration. As the morphological steps of oral apparatus formation and strikingly similar between regeneration and cell division, this suggests the possibility that oral regeneration might be using parts of the cell cycle machinery to regulate timing of events. Because E2F knockdown leads to a delay or failure of late stages of regeneration, this may reflect a role of cell cycle related E2F targets in this system. The phenotype from E2F RNAi regeneration experiments may be from reduced progression through cell cycle transitions associated with successive steps of regeneration. To determine which cell cycle transitions might align with steps of regeneration, we compared a list of *Stentor* genes compared with human cell cycle genes [8] to the list of genes differentially expressed in 2HPS Palbociclib treated cells. Because we expect the cells to be in the "preparatory" state at 2HPS, this could act similar to a transition in the cell cycle. In these cells where the E2F pathway is inhibited through CDK4/6, a number of S phase genes were upregulated and G2M genes were downregulated. Thus, in normal regenerating cells at 2HPS, this may represent a transition from S to G2 phases of the cell cycle. This is consistent with non-morphogenic cells being in a constant state of interphase until cell division when it exits S phase and enters into G2 and mitosis.

Later in regeneration, Aurora kinases are upregulated, and their inhibition also delays regeneration, but at a later step [10]. Aurora kinase signaling indicates that a spindle is properly assembled, and a similar mechanism could be in play in *Stentor* to signal the correct assembly of one or more structures during regeneration. Regeneration, like cell division, might require a series of checkpoints, one of which is mediated by E2F signaling and another by Aurora kinase signaling. This suggests that regeneration may be using cell cycle machinery to regulate the timing of regeneration.

Another possibility for why cell cycle genes are seen in *Stentor* regeneration is that micronuclei undergo mitotic division during regeneration as well. It could be that the expression of cell cycle and mitosis genes during regeneration occurs simply because the micronuclei divide in this process. However, micronuclei are not required for regeneration, and E2F knockdowns and Palbociclib treated cells have regeneration defects, indicating that these cell cycle genes are likely upregulated for the process of regeneration rather than micronuclei division.

Triggers for regeneration and activation state

In Tartar's experiments, grafting cells in a regenerating "state" into large non-regenerating cells can be enough to drive the large cell into division [2]. This shows that the activated state can be spread to another cell, whether through the cytoplasm or the cortex. Presumably the large non-regenerating cell is in a state of inhibition, however, the activation state from the regenerating cell is often enough to push the non-regenerating cell into division. The activating state for morphogenesis thus applies to

both regeneration and cell division. If the sender-receiver model is occurring in this situation, and if there is a beacon signal that inhibits regeneration, what is this signal? If an inhibitory signal exists in the large non-regenerating cell which normally suppresses oral primordium formation, then the activation state from the regenerating cell must override or neutralize this signal. Identifying the nature of this beacon is a key question. It may involve spatial cues in the cortex, inhibitory kinases, or physical continuity in the cytoskeleton that suppress morphogenetic initiation.

Downstream of this hypothetical inhibition-release mechanism, candidate effectors include cell cycle regulators such as CDK4/Cyclin D, which are known to govern G1/S phase transition. This suggests that signals controlling development can also activate the cell cycle, connecting regeneration to cell division. The grafting experiments hint that the reprogramming of the recipient cell may involve not only localized structural reorganization but also a molecular shift into a proliferative state. This grafting paradigm thus offers a compelling biological system to dissect the molecular nature of activation, the trigger for morphogenesis, and the interface between patterning and proliferation.

Further work could involve identifying candidate signaling molecules in the activated cytoplasm and investigating MAPK signaling, which may act upstream of CDK4/Cyclin and may reveal candidate effectors in the sender-receiver model for oral primordium development.

E2F and other multi-ciliated cell types

A transcriptomic profile of vegetative cell division was done in another ciliate, *Tetrahymena thermophila,* and revealed major drivers of the eukaryotic cell cycle progression including cyclins, CDKs and E2F transcription factors [84]. *Tetrahymena* cells have a meiosis specific E2F [85] as well as 2 inhibitory, 2 activating, and one atypical E2F [84]. In *Stentor*, there are 23 different E2F isoforms, some of which may be redundant. The temporal expression of E2F2 and E2F4 in *Tetrahymena* shows that they peak early in the process of cell division, similar to the E2F in this study, SteCoe_12750 in regeneration. While we cannot determine whether SteCoe_12750 is an activating or repressing E2F, its sequence is most homologous to E2F2 in *Tetrahymena*, based on its conserved winged-helix DNA-binding.

In epithelial multi-ciliated cell systems where hundreds of motile cilia per cell produce fluid flow, these differentiating cells undergo a form of centriole assembly and maturation that produces hundreds of mother centrioles and thus basal bodies which are required for cilia extension. Multicilin, a small coiled-coil protein, is shown to form a ternary complex with E2f4 and Dp1 and activates most of the genes required for centriole biogenesis while other cell cycle genes remain off [86]. E2f4 acts as a repressor of cell cycle genes and regulates genes required for centriole assembly during cell division [87]. Multicilin co-opts the inhibitory E2fs to activate key components that drive centriole assembly during the centriolar cycle [86]. Although Multicilin is only present in a subset of vertebrate species, it could be just one example of a transcriptional coregulator that evolved to co-opt an existing transcriptional factor complex to coordinate the regulation of a large number of genes required for multiciliogenesis.

Cell cycle and cancer

Regeneration, cancer, and the cell cycle are deeply intertwined processes that revolve around a cell's ability to control growth, proliferation and pattern formation. Understanding how the cell cycle is re-engaged during regeneration but mis-regulated in cancer reveals shared principles governing plasticity, control and fate. Loss of cell cycle control is a hallmark of cancer, which can be targeted with agents including cyclin dependent kinase 4/6 (CDK4/6) kinase inhibitors that act on the G1/S cell cycle checkpoint by maintaining Rb activity and thus repressing uncontrolled cell cycle progression. While regeneration involves many of the same players such as E2F, CDK4/CyclinD and Rb, it uses transient and regulated expression of these factors, where it uses similar proliferative machinery but with strict and regulated control. Understanding how organisms capable of regeneration control regenerative responses without triggering tumorigenesis may reveal strategies for stimulating repair in tissues and cells while avoiding cancerous or uncontrolled cell proliferation. If non-regenerating cells contain the machinery for regeneration, can we harness this in a way to turn these cells into ones with regenerative capacity?

3.5 Materials and Methods

Stentor culture and Regeneration Assay

Stentor coeruleus cells were obtained from Carolina Biological Supply and grown in the dark, at room temperature in the lab. Cells are cultured in pasteurized spring water (Carolina Biological Supply). Cells are fed every 4-5 days with *Chlamydomonas reinhardtii* grown on TAP agar plates and resuspended in 15mL pasteurized spring water, with each 2-quart culture being fed 5mL.

Regeneration assays were performed as previously described [89]. Briefly, cells were placed in a 30% sucrose solution until the membranellar bands had fallen off, approximately 1.5 minutes. Cells were washed 3x with Carolina Spring water and staged at 8HPS, where stage 1 indicates a bald stentor, stage 2 has an oral primordium, stage 3 has a gullet, and stage 4 is fully regenerated.

Palbociclib experiments

In initial drug treatment experiments, sucrose shocked cells were incubated in 5uM Palbociclib and allowed to regenerate for 8 hours. In washout experiments, sucrose shocked cells were incubated in 5uM Palbociclib for 4 hours and then washed 3x with pasteurized spring water (Carolina Biological Supply) and allowed to regenerate for another 4 hours. Spike in experiments were performed similarly, with Palbociclib added at 0HPS, 4HPS and 6HPS.

Edu Incorporation Assay

Either vegetative cells or cells at timepoints during regeneration were fixed in freezing methanol (Sigma Aldrich) and washed with PBST. Click-iT EdU Cell Proliferation Kit (Invitrogen C10337) was used according to the manufacturer's protocol to look at synthesizing DNA. 10uM of Edu was used per sample. Total DNA was visualized using Hoescht 33342.

RNA sequencing

Cells were pre-treated with 5uM Palbociclib for 1 hour, washed 3x with Pasteurized Spring water (Carolina Biological). They were sucrose-shocked in 30% sucrose for 1:30 minutes or until the membranellar bands had fallen off. Cells were washed again and incubated in 5uM Palbociclib. After 2HPS, cells were placed in Trizol (Invitrogen 15596026). RNA was extracted using a PureLink RNA Mini Kit (Invitrogen) and libraries were prepped using the NEBNext Ultra II RNA Library Prep Kit (New England BioLabs) following manufacturer's instructions. Samples were pooled and submitted for sequencing on an Illumina NovaSeqX (SP300). We used kallisto[90] to generate a reference index and quantify transcript abundance and sleuth[91] to perform differential enrichment analysis.

Phosphoproteomics

Cells were pre-treated with Palbociclib for 1 hours, washed 3x with Pasteurized Spring water (Carolina Biological) and sucrose shocked in 30% until the membranellar bands had fallen off. Cells were washed again and incubated in 5uM Palbociclib for 1 hour. Cells were washed to remove Palbociclib, and volume was reduced to 50uL. Roche PhosSTOP Phosphatase inhibitor (Millipore Sigma) was added at 1% and cells were frozen using an ethanol dry ice bath and stored in-80C until samples were shipped.

Imaging

Brightfield imaging was done using Zeiss AxioZoom V16 equipped with a Nikon Rebel T3i SLR Camera. Confocal immunofluorescence microscopy was done using CSU-WI Spinning disk equipped with an Andor Zyla sCMOS camera. Confocal microscopy of Edu incorporation was performed on an IN Cell Analyzer 6000.

CHAPTER 4: DISSERTATION DISCUSSION

4.1 Sfi1's role in centrin patterning and regeneration

This dissertation highlights a previously uncharacterized role for Sfi1 proteins in the regulation of the centrin based cytoskeleton and scaffolding of the oral primordium during oral regeneration in *Stentor*. Sfi1, a conserved centrin binding protein best known for its role in spindle pole duplication in yeast [38] appears to play a key structural and regulatory role in *Stentor*'s unique cortical architecture. We found that Sfi1 localizes to distinct lateral structures that partially overlap with centrin fibers in the posterior. Because Sfi1 localizes to regions without centrin, this suggests that Sfi1 is not simply a scaffold but may mark zones of cortical differentiation. The regionalized distribution of Sfi1 along the anterior-posterior axis further supports the idea that different cortical regions utilize distinct cytoskeletal modules, possibly reflecting functional compartmentalization related to polarity. The sequential scaffolding model presented in this study suggests that Sfi1 proteins are not just passive structural components but are active participants in the building of an oral apparatus, which potentially links cytoskeletal patterning, polarity, and regeneration in *Stentor*.

4.2 Future directions in the study of regeneration triggers

Our findings implicate the E2F pathway as part of the early regenerative program in Stentor. The expression of E2F and its targets during regeneration suggests that E2F may have broader roles beyond C1/S cell cycle progression. However, many questions remain about the upstream regulation, functional targets and mechanistic roles of E2F in the context of regeneration. Because we have identified a potential upstream regulator of CDK4/Cyclin D, we can test using pharmacological inhibition using MEK inhibitors to see if MAPK signaling is indeed regulating CDK4/CyclinD in regeneration. Additionally, follow-up experiments include RNA sequencing of E2F RNAi knockdowns at early timepoints to see if the results match our Palbociclib RNA sequencing results, and to identify genes that are targets of E2F. E2F stands at an intersection of cell cycle regulation and regenerative morphogenesis in Stentor. Futures work will need to clarify whether E2F is simply co-opted for transcriptional activation during regeneration, or whether it serves as a master regulator integrating injury signals with regeneration programs. Unraveling this will advance our understanding of not only unicellular regeneration, but also of how cell cycle machinery can be repurposed for non-proliferative outcomes across evolution.

REFERENCES

[1] E. M. De Robertis, “Wnt signaling in axial patterning and regeneration: lessons from planaria,” *Sci Signal*, vol. 3, no. 127, p. pe21, Jun. 2010, doi: 10.1126/scisignal.3127pe21.

[2] V. Tartar, *The biology of Stentor*. New York, Pergammon Press, 1961.

[3] W. F. Marshall, “Regeneration in Stentor coeruleus,” *Front Cell Dev Biol*, vol. 9, p. 753625, 2021, doi: 10.3389/fcell.2021.753625.

[4] D. C. Wood, “Habituation in Stentor: a response-dependent process,” *J Neurosci*, vol. 8, no. 7, pp. 2248–2253, Jul. 1988, doi: 10.1523/JNEUROSCI.08-07-02248.1988.

[5] L. H. Bannister and E. C. Tatchell, “Contractility and the fibre systems of Stentor Coeruleus,” *Journal of Cell Science*, vol. 3, no. 2, pp. 295–308, Jun. 1968, doi: 10.1242/jcs.3.2.295.

[6] T. H. Morgan, “Regeneration of proportionate structures in stentor,” *The Biological Bulletin*, vol. 2, no. 6, pp. 311–328, Jun. 1901, doi: 10.2307/1535709.

[7] V. Tartar, “Grafting experiments concerning primordium formation in Stentor coeruleus,” *Journal of Experimental Zoology*, vol. 131, no. 1, pp. 75–121, 1956, doi: 10.1002/jez.1401310105.

[8] P. Sood *et al.*, “Modular, cascade-like transcriptional program of regeneration in Stentor,” *eLife*, vol. 11, p. e80778, Aug. 2022, doi: 10.7554/eLife.80778.

[9] A. Lin *et al.*, “Determining protein polarization proteome-wide using physical dissection of individual Stentor coeruleus cells,” *Curr Biol*, vol. 32, no. 10, pp. 2300-2308.e4, May 2022, doi: 10.1016/j.cub.2022.03.078.

[10] A. Lin, D. Summers, S. B. Reiff, A. R. Tipton, S. K. Tang, and W. F. Marshall, “Aurora kinase inhibitors delay regeneration in Stentor coeruleus at an intermediate step,” *Matters Sel*, vol. 6, no. 4, p. 202003000006, 2020.

[11] H. Onsbring, M. Jamy, and T. J. G. Ettema, “RNA Sequencing of Stentor Cell Fragments Reveals Transcriptional Changes during Cellular Regeneration,” *Curr Biol*, vol. 28, no. 8, pp. 1281-1288.e3, Apr. 2018, doi: 10.1016/j.cub.2018.02.055.

[12] M. M. Slabodnick *et al.*, “The macronuclear genome of Stentor coeruleus reveals tiny introns in a giant cell,” *Curr Biol*, vol. 27, no. 4, pp. 569–575, Feb. 2017, doi: 10.1016/j.cub.2016.12.057.

[13] N. De Terra, MACRONUCLEAR DNA SYNTHESIS IN Stentor: REGULATION BY A CYTOPLASMIC INITIATOR*, Proc. Natl. Acad. Sci. U.S.A. 57 (3) 607-614, https://doi.org/10.1073/pnas.57.3.607 (1967).

[14] L. Zhang, M. D. Cervantes, S. Pan, J. Lindsley, A. Dabney, and G. M. Kapler, “Transcriptome analysis of the binucleate ciliate Tetrahymena thermophila with asynchronous nuclear cell cycles,” *MBoC*, vol. 34, no. 2, p. rs1, Feb. 2023, doi: 10.1091/mbc.E22-08-0326.

[15] K. J. Aufderheide, J. Frankel, and N. E. Williams, “Formation and positioning of surface-related structures in protozoa,” *Microbiological Reviews*, vol. 44, no. 2, pp. 252–302, Jun. 1980, doi: 10.1128/mr.44.2.252-302.1980.

[16] J. Frankel, *Pattern Formation: Ciliate Studies and Models*. Oxford University Press, 1989.

[17] R. Li and G. G. Gundersen, “Beyond polymer polarity: how the cytoskeleton builds a polarized cell,” *Nat Rev Mol Cell Biol*, vol. 9, no. 11, pp. 860–873, Nov. 2008, doi: 10.1038/nrm2522.

[18] A. R. Albright, C. Yan, D. Angeles-Albores, T. Makushok, J. Allen-Henderson, and W. F. Marshall, “Genome-wide analysis of anterior-posterior mRNA regionalization in Stentor coeruleus reveals a role for the microtubule cytoskeleton,” Oct. 08, 2024, *bioRxiv*. doi: 10.1101/2023.01.09.523364.

[19] H. S. Jennings, “Studies on reactions to stimuli in unicellular organisms. ix.—on the behavior of fixed infusoria (stentor and vorticella), with special reference to the modifiability of protozoan reactions,” *American Journal of Physiology-Legacy Content*, vol. 8, no. 1, pp. 23–60, Oct. 1902, doi: 10.1152/ajplegacy.1902.8.1.23.

[20] J. T. Randall and S. F. Jackson, “Fine structure and function in Stentor polymorphous,” *J Biophys Biochem Cytol*, vol. 4, no. 6, pp. 807–830, Nov. 1958, doi: 10.1083/jcb.4.6.807.

[21] Fauré-Fremiet, Myonèmes et cinétodesmes chez les ciliés du genre Stentor, *Bull. Microsc. Appl.*, 8, 117-119 1958

[22] M. S. Maloney, W. S. McDaniel, S. A. Locknar, and H. M. Torlina, “Identification and localization of a protein immunologically related to Caltractin (Centrin) in the Myonemes and Membranelles of the Heterotrich ciliate Stentor coeruleus,” *J Eukaryot Microbiol*, vol. 52, no. 4, pp. 328–338, 2005, doi: 10.1111/j.1550-7408.2005.00048x.

[23] L. Chen and K. Madura, “Centrin/Cdc31 is a novel regulator of protein degradation,” *Mol Cell Biol*, vol. 28, no. 5, pp. 1829–1840, Mar. 2008, doi: 10.1128/MCB.01256-07.

[24] T. Fischer, S. Rodríguez-Navarro, G. Pereira, A. Rácz, E. Schiebel, and E. Hurt, “Yeast centrin Cdc31 is linked to the nuclear mRNA export machinery,” *Nat Cell Biol*, vol. 6, no. 9, pp. 840–848, Sep. 2004, doi: 10.1038/ncb1163.

[25] R. Nishi, W. Sakai, D. Tone, F. Hanaoka, and K. Sugasawa, “Structure-function analysis of the EF-hand protein centrin-2 for its intracellular localization and nucleotide excision repair,” *Nucleic Acids Res*, vol. 41, no. 14, pp. 6917–6929, Aug. 2013, doi: 10.1093/nar/gkt434.

[26] A. Paoletti, M. Moudjou, M. Paintrand, J. L. Salisbury, and M. Bornens, “Most of centrin in animal cells is not centrosome-associated and centrosomal centrin is confined to the distal lumen of centrioles,” *Journal of Cell Science*, vol. 109, no. 13, pp. 3089–3102, Dec. 1996, doi: 10.1242/jcs.109.13.3089.

[27] K. K. Resendes, B. A. Rasala, and D. J. Forbes, “Centrin 2 localizes to the vertebrate nuclear pore and plays a role in mRNA and protein export,” *Mol Cell Biol*, vol. 28, no. 5, pp. 1755–1769, Mar. 2008, doi: 10.1128/MCB.01697-07.

[28] C.-H. Yang, C. Kasbek, S. Majumder, A. M. Yusof, and H. A. Fisk, “Mps1 phosphorylation sites regulate the function of centrin 2 in centriole assembly,” *Mol Biol Cell*, vol. 21, no. 24, pp. 4361–4372, Dec. 2010, doi: 10.1091/mbc.E10-04-0298.

[29] R. Basto *et al.*, “Flies without centrioles,” *Cell*, vol. 125, no. 7, pp. 1375–1386, Jun. 2006, doi: 10.1016/j.cell.2006.05.025.

[30] Fauré-Fremiet, E., Ch Rouiller, and M. Gauchery. "Les structures myoides chez les ciliés. Etude au microscope électronique." *Arch. Anat. Microsc. Morphol. Exp* 45 (1956): 139.

[31] Inaba, R. "Electron-microscope study on the fine structure of Stentor coeruleus." *Bull. Biol. Soc. Hiroshima Univ* 10 (1961): 35.

[32] N. Garreau de Loubresse, G. Keryer, B. Vigues, and J. Beisson, “A contractile cytoskeleton network of Paramecium: The infraciliary lattice,” *J Cell Sci*, no. 90, pp. 351–364, 1988.

[33] W. Amos and L. Routledge, “Calcium-binding proteins in a Volticellid contractile organelle,” *J Cell Sci*, vol. 19, pp. 203–213, 1975.

[34] B. Huang and D. Mazia, “Microtubules and filaments in ciliate contractility,” *Soc Gen Physiol Ser*, vol. 30, pp. 389–409, 1975.

[35] B. Huang and D. R. Pitelka, “THE CONTRACTILE PROCESS IN THE CILIATE, *STENTOR COERULEUS*,” *The Journal of Cell Biology*, vol. 57, no. 3, pp. 704–728, Jun. 1973, doi: 10.1083/jcb.57.3.704.

[36] T. Weis-Fogh and W. B. Amos, “Evidence for a new mechanism of cell motility,” *Nature*, vol. 236, no. 5345, pp. 301–304, Apr. 1972, doi: 10.1038/236301a0.

[37] J. J. Maciejewski, E. J. Vacchiano, S. M. Mccutcheon, and H. E. Buhse Jr., “Cloning and Expression of a cDNA Encoding a Vorticella convallaria Spasmin: an EF-Hand Calcium-Binding Protein,” *Journal of Eukaryotic*

Microbiology, vol. 46, no. 2, pp. 165–173, 1999, doi: 10.1111/j.1550-7408.1999.tb04601.x.

[38] J. V. Kilmartin, "Sfi1p has conserved centrin-binding sites and an essential function in budding yeast spindle pole body duplication," *J Cell Biol*, vol. 162, no. 7, pp. 1211–1221, Sep. 2003, doi: 10.1083/jcb.200307064.

[39] S. Li, A. M. Sandercock, P. Conduit, C. V. Robinson, R. L. Williams, and J. V. Kilmartin, "Structural role of Sfi1p–centrin filaments in budding yeast spindle pole body duplication," *J Cell Biol*, vol. 173, no. 6, pp. 867–877, Jun. 2006, doi: 10.1083/jcb.200603153.

[40] D. Gogendeau *et al.*, "An Sfi1p-like centrin-binding protein mediates centrin-based Ca2+ -dependent contractility in Paramecium tetraurelia," *Eukaryot Cell*, vol. 6, no. 11, pp. 1992–2000, Nov. 2007, doi: 10.1128/EC.00197-07.

[41] D. Gogendeau *et al.*, "Functional diversification of centrins and cell morphological complexity," *J Cell Sci*, vol. 121, no. Pt 1, pp. 65–74, Jan. 2008, doi: 10.1242/jcs.019414.

[42] A. J. Stemm-Wolf, J. B. Meehl, and M. Winey, "Sfr13, a member of a large family of asymmetrically localized Sfi1-repeat proteins, is important for basal body separation and stability in Tetrahymena thermophila," *J Cell Sci*, vol. 126, no. 7, pp. 1659–1671, Apr. 2013, doi: 10.1242/jcs.120238.

[43] W. Heydeck, A. J. Stemm-Wolf, J. Knop, C. C. Poh, and M. Winey, "Sfr1, a Tetrahymena thermophila Sfi1 Repeat Protein, Modulates the Production of Cortical Row Basal Bodies," *mSphere*, vol. 1, no. 6, pp. e00257-16, 2016, doi: 10.1128/mSphere.00257-16.

[44] J. Zhang *et al.*, “Giant proteins in a giant cell: Molecular basis of ultrafast Ca2+-dependent cell contraction,” *Science Advances*, vol. 9, no. 8, p. eadd6550, Feb. 2023, doi: 10.1126/sciadv.add6550.

[45] J. Lannan *et al.*, “Fishnet mesh of centrin-Sfi1 drives ultrafast calcium-activated contraction of the giant cell Spirostomum ambiguum,” *bioRxiv*, p. 2024.11.07.622534, Nov. 2024, doi: 10.1101/2024.11.07.622534.

[46] E. Newman, “Contraction in Stentor coeruleus: A Cinematic Analysis,” *Science*, vol. 177, no. 47, pp. 447–449, Aug. 1972.

[47] S. Prowazrek, “Beitrag zur Kenntnis der Regeneration and Biologic der Protozoan,” *Arch. Protistenk*, vol. 3, pp. 44–59, 1904.

[48] A. Aubusson-Fleury, G. Balavoine, M. Lemullois, K. Bouhouche, J. Beisson, and F. Koll, “Centrin diversity and basal body patterning across evolution: new insights from Paramecium,” *Biol Open*, vol. 6, no. 6, pp. 765–776, Jun. 2017, doi: 10.1242/bio.024273.

[49] M. Pedretti, L. Bombardi, C. Conter, F. Favretto, P. Dominici, and A. Astegno, “Structural Basis for the Functional Diversity of Centrins: A Focus on Calcium Sensing Properties and Target Recognition,” *Int J Mol Sci*, vol. 22, no. 22, p. 12173, Nov. 2021, doi: 10.3390/ijms222212173.

[50] K. Konior, S. M. McCUTCHEON, and H. E. BUHSE Jr., “Characterization of Vorticella convallaria calcium-binding centrin proteins,” *Journal of Eukaryotic Microbiology*, vol. 52, no. 2, pp. 7S-27S, 2005, doi: 10.1111/j.1550-7408.2005.05202003_1_43.x.

[51] A. Heger and L. Holm, “Rapid automatic detection and alignment of repeats in protein sequences,” *Proteins*, vol. 41, no. 2, pp. 224–237, Nov. 2000, doi: 10.1002/1097-0134(20001101)41:2<224::aid-prot70>3.0.co;2-z.

[52] E. de Castro *et al.*, “ScanProsite: detection of PROSITE signature matches and ProRule-associated functional and structural residues in proteins,” *Nucleic Acids Research*, vol. 34, no. suppl_2, pp. W362–W365, Jul. 2006, doi: 10.1093/nar/gkl124.

[53] J. Abramson *et al.*, “Accurate structure prediction of biomolecular interactions with AlphaFold 3,” *Nature*, vol. 630, no. 8016, pp. 493–500, Jun. 2024, doi: 10.1038/s41586-024-07487-w.

[54] A. Klimas *et al.*, “Magnify is a universal molecular anchoring strategy for expansion microscopy,” *Nat Biotechnol*, vol. 41, no. 6, pp. 858–869, Jun. 2023, doi: 10.1038/s41587-022-01546-1.

[55] W. Wei, C. Jiang, W. Yang, W. Miao, and J. Xiong, “Proteomic identification and expression of oral apparatus constituents in cell regeneration of giant ciliate *Stentor coeruleus* (strain WHEL),” *Gene*, vol. 743, p. 144624, Jun. 2020, doi: 10.1016/j.gene.2020.144624.

[56] N. De Terra, “Cytoskeletal discontinuities in the cell body cortex initiate basal body assembly and oral development in the ciliate Stentor,” *Development*, vol. 87, no. 1, pp. 249–257, Jun. 1985, doi: 10.1242/dev.87.1.249.

[57] M. S. Maloney, “Pharmacological evidence for cell surface control of oral regeneration in Stentor coeruleus,” *Journal of Cellular Physiology*, vol. 103, no. 2, pp. 305–311, 1980, doi: 10.1002/jcp.1041030216.

[58] W. Qin *et al.*, “Dynamic shape-shifting of the single-celled eukaryotic predator *Lacrymaria* via unconventional cytoskeletal components,” *Current Biology*, vol. 34, no. 21, pp. 4869-4883.e6, Nov. 2024, doi: 10.1016/j.cub.2024.09.003.

[59] D. Zhou, S. Lambert, P. L. Malen, S. Carpenter, L. M. Boland, and V. Bennett, “AnkyrinG is required for clustering of voltage-gated Na channels at axon initial segments and for normal action potential firing,” *J Cell Biol*, vol. 143, no. 5, pp. 1295–1304, Nov. 1998, doi: 10.1083/jcb.143.5.1295.

[60] K. L. Hedstrom, Y. Ogawa, and M. N. Rasband, “AnkyrinG is required for maintenance of the axon initial segment and neurona l polarity,” *Journal of Cell Biology*, vol. 183, no. 4, pp. 635–640, Nov. 2008, doi: 10.1083/jcb.200806112.

[61] A. Villalobo, H. Ishida, H. J. Vogel, and M. W. Berchtold, “Calmodulin as a protein linker and a regulator of adaptor/scaffold proteins,” *Biochim Biophys Acta Mol Cell Res*, vol. 1865, no. 3, pp. 507–521, Mar. 2018, doi: 10.1016/j.bbamcr.2017.12.004.

[62] M. S. Maloney, P. R. Walsh, and K. B. Rhoadarmer, “Calcium And Calmodulin Antagonists Delay Oral Regeneration In The Ciliate Stentor Coeruleus,” *Journal of Experimental Biology*, vol. 161, no. 1, pp. 135–149, Nov. 1991, doi: 10.1242/jeb.161.1.135.

[63] Y. E. Xuwen, Z. Wenlong, W. Zhijun, Z. Yaqin, and Y. Binsheng, “Binding of Trifluoperazine to N-terminal Domain of Euplotes Octocarinatus Centrin and the Influence on Its Function †,” *Chemical Journal of Chinese Universities*, vol. 40, no. 11, p. 2257, Nov. 2019, doi: 10.7503/cjcu20190334.

[64] M. K. Showe and L. W. Black, “Assembly Core of Bacteriophage T4: an Intermediate in Head Formation,” *Nature New Biology*, vol. 242, no. 116, pp. 70–75, Mar. 1973, doi: 10.1038/newbio242070a0.

[65] D. Kressler, E. Hurt, and J. Baβler, “Driving ribosome assembly,” *Biochimica et Biophysica Acta (BBA) - Molecular Cell Research*, vol. 1803, no. 6, pp. 673–683, Jun. 2010, doi: 10.1016/j.bbamcr.2009.10.009.

[66] S. M. Cohen, “Specification of limb development in the Drosophila embryo by positional cues from segmentation genes,” *Nature*, vol. 343, no. 6254, pp. 173–177, Jan. 1990, doi: 10.1038/343173a0.

[67] H. Bohn, “Interkalare Regeneration und segmentale Gradienten bei den Extremitäten von Leucophaea-Larven (Blattaria),” *Wilhelm Roux’ Arch. EntwMech.*, vol. 165, pp. 303–341, 1970.

[68] S. F. Altschul, W. Gish, W. Miller, E. W. Myers, and D. J. Lipman, “Basic local alignment search tool,” *J Mol Biol*, vol. 215, no. 3, pp. 403–410, Oct. 1990, doi: 10.1016/S0022-2836(05)80360-2.

[69] B. Q. Minh *et al.*, “IQ-TREE 2: New Models and Efficient Methods for Phylogenetic Inference in the Genomic Era,” *Mol Biol Evol*, vol. 37, no. 5, pp. 1530–1534, May 2020, doi: 10.1093/molbev/msaa015.

[70] D. T. Hoang, O. Chernomor, A. von Haeseler, B. Q. Minh, and L. S. Vinh, “UFBoot2: Improving the Ultrafast Bootstrap Approximation,” *Mol Biol Evol*, vol. 35, no. 2, pp. 518–522, Feb. 2018, doi: 10.1093/molbev/msx281.

[71] S. Guindon and O. Gascuel, “A simple, fast, and accurate algorithm to estimate large phylogenies by maximum likelihood,” *Syst Biol*, vol. 52, no. 5, pp. 696–704, Oct. 2003, doi: 10.1080/10635150390235520.

[72] M. M. Slabodnick, J. G. Ruby, J. G. Dunn, J. L. Feldman, J. L. DeRisi, and W. F. Marshall, “The Kinase Regulator Mob1 Acts as a Patterning Protein for Stentor Morphogenesis,” *PLOS Biology*, vol. 12, no. 5, p. e1001861, May 2014, doi: 10.1371/journal.pbio.1001861.

[73] M. Slabodnick, B. Prevo, P. Gross, J. Sheung, and W. Marshall, “Visualizing cytoplasmic flow during single-cell wound healing in Stentor coeruleus,” *J Vis Exp*, no. 82, p. e50848, Dec. 2013, doi: 10.3791/50848.

[74] D. J. Guerin, C. X. Kha, and K. A.-S. Tseng, “From Cell Death to Regeneration: Rebuilding After Injury,” *Front. Cell Dev. Biol.*, vol. 9, Mar. 2021, doi: 10.3389/fcell.2021.655048.

[75] A. A. Aboobaker, “Planarian stem cells: a simple paradigm for regeneration,” *Trends in Cell Biology*, vol. 21, no. 5, pp. 304–311, May 2011, doi: 10.1016/j.tcb.2011.01.005.

[76] C. M. Child, “Patterns and Problems of Development,” *Univ. of Chicago Press*, p. p811, 1941.

[77] S. M. Rose, “Electrical studies on normally regenerating, on X-rayed and on denervated limb stumps on Triturus,” *Appleton-Century-Crofts*, p. 264, 1972.

[78] I. Kovesdi, M. Satake, K. Furukawa, R. Reichel, Y. Ito, and J. R. Nevins, “A factor discriminating between the wildtype and a mutant polyomavirus enhancer,” *Nature*, vol. 328, no. 6125, pp. 87–89, Jul. 1987, doi: 10.1038/328087a0.

[79] N. B. La Thangue and P. W. Rigby, “An adenovirus E1A-like transcription factor is regulated during the differentiation of murine embryonal carcinoma

stem cells," *Cell*, vol. 49, no. 4, pp. 507–513, May 1987, doi: 10.1016/0092-8674(87)90453-3.

[80] A. S. Yee, R. Reichel, I. Kovesdi, and J. R. Nevins, "Promoter interaction of the E1A-inducible factor E2F and its potential role in the formation of a multi-component complex," *EMBO J*, vol. 6, no. 7, pp. 2061–2068, Jul. 1987, doi: 10.1002/j.1460-2075.1987.tb02471.x.

[81] W. Driever and C. Nüsslein-Volhard, "The bicoid protein determines position in the Drosophila embryo in a concentration-dependent manner," *Cell*, vol. 54, no. 1, pp. 95–104, Jul. 1988, doi: 10.1016/0092-8674(88)90183-3.

[82] S. B. Reiff and W. F. Marshall, "A large kinome in a large cell: Stentor coeruleus possesses highly expanded kinase families and novel domain architectures," Jul. 25, 2017, *bioRxiv*. doi: 10.1101/168187.

[83] M. Cargnello and P. P. Roux, "Activation and Function of the MAPKs and Their Substrates, the MAPK-Activated Protein Kinases," *Microbiol Mol Biol Rev*, vol. 75, no. 1, pp. 50–83, Mar. 2011, doi: 10.1128/MMBR.00031-10.

[84] L. Zhang, M. D. Cervantes, S. Pan, J. Lindsley, A. Dabney, and G. M. Kapler, "Transcriptome analysis of the binucleate ciliate Tetrahymena thermophila with asynchronous nuclear cell cycles," *MBoC*, vol. 34, no. 2, p. rs1, Feb. 2023, doi: 10.1091/mbc.E22-08-0326.

[85] J. Zhang, M. Tian, G.-X. Yan, A. Shodhan, and W. Miao, "E2fl1 is a meiosis-specific transcription factor in the protist Tetrahymena thermophila," *Cell Cycle*, vol. 16, no. 1, pp. 123–135, Jan. 2017, doi: 10.1080/15384101.2016.1259779.

[86] L. Ma, I. Quigley, H. Omran, and C. Kintner, “Multicilin drives centriole biogenesis via E2f proteins,” *Genes Dev.*, vol. 28, no. 13, pp. 1461–1471, Jul. 2014, doi: 10.1101/gad.243832.114.

[87] M. E. Crosby and A. Almasan, “Opposing roles of E2Fs in cell proliferation and death,” *Cancer Biol Ther*, vol. 3, no. 12, pp. 1208–1211, Dec. 2004, doi: 10.4161/cbt.3.12.1494.

[88] F. Serra, P. Lapidari, E. Quaquarini, B. Tagliaferri, F. Sottotetti, and R. Palumbo, “Palbociclib in metastatic breast cancer: current evidence and real-life data,” *Drugs Context*, vol. 8, p. 212579, Jul. 2019, doi: 10.7573/dic.212579.

[89] A. Lin, T. Makushok, U. Diaz, and W. F. Marshall, “Methods for the Study of Regeneration in Stentor,” *JoVE (Journal of Visualized Experiments)*, no. 136, p. e57759, Jun. 2018, doi: 10.3791/57759.

[90] N. L. Bray, H. Pimentel, P. Melsted, and L. Pachter, “Near-optimal probabilistic RNA-seq quantification,” *Nat Biotechnol*, vol. 34, no. 5, pp. 525–527, May 2016, doi: 10.1038/nbt.3519.

[91] H. Pimentel, N. L. Bray, S. Puente, P. Melsted, and L. Pachter, “Differential analysis of RNA-seq incorporating quantification uncertainty,” *Nat Methods*, vol. 14, no. 7, pp. 687–690, Jul. 2017, doi: 10.1038/nmeth.4324.

Publishing Agreement

It is the policy of the University to encourage open access and broad distribution of all theses, dissertations, and manuscripts. The Graduate Division will facilitate the distribution of UCSF theses, dissertations, and manuscripts to the UCSF Library for open access and distribution. UCSF will make such theses, dissertations, and manuscripts accessible to the public and will take reasonable steps to preserve these works in perpetuity.

I hereby grant the non-exclusive, perpetual right to The Regents of the University of California to reproduce, publicly display, distribute, preserve, and publish copies of my thesis, dissertation, or manuscript in any form or media, now existing or later derived, including access online for teaching, research, and public service purposes.

DocuSigned by:
Connie Yan
09D23A9CE3904F6...
Author Signature

7/21/2025
Date